Master Thesis

on

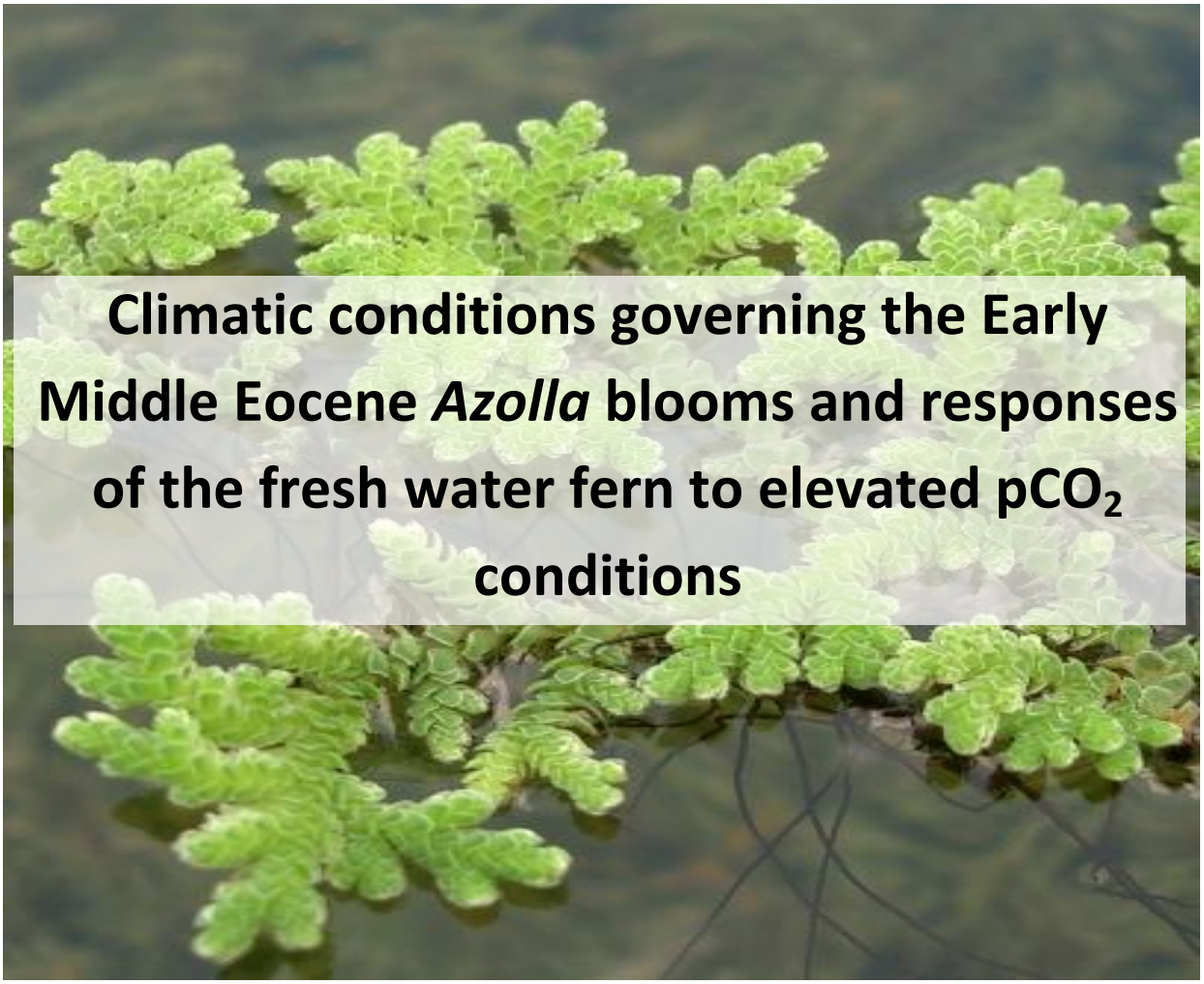

Climatic conditions governing the Early Middle Eocene *Azolla* blooms and responses of the fresh water fern to elevated pCO_2 conditions

By Rolande Dekker

Utrecht University
Department of Earth Sciences
Organic geochemistry
December 2010
R.Dekker6@students.uu.nl

Supervised by

Eveline N. Speelman

Gert-Jan Reichart

Contents

Part 1 Climatic conditions governing extensive *Azolla* blooms during the Middle Eocene

1 Introduction
2 Background information
- 2.1 Geochemically reconstructing sea surface temperatures
- 2.2 Geochemically reconstructing Eocene Arctic precipitation

3 Materials and methods
- 3.1 Sample material
- 3.2 Methods

4 Results and discussion
- 4.1 Temperatures in the Eocene Arctic basin
- 4.2 Latitudinal temperature gradient in de Eocene
- 4.3 Eocene Hydrological cycle reconstruction
- 4.4 Eocene Arctic sea surface mixing and salinity

5 Conclusion

Appendices
- A1 GDGT structures, TEX_{86} algorithm and BIT-index
- A2 Comparing TEX_{86} calibrations
- A3 Other compound occurrence

References

Part 2 Physiological and carbon isotopic responses of the freshwater fern *Azolla* to elevated pCO_2 conditions

1 Introduction
2 Materials and methods
- 2.1 Sample material
- 2.2 Methods – experimental set-up

3 Results and discussion
- 3.1 Growth rate at elevated CO_2 conditions
- 3.2 Bulk TOC and N_{tot} measurements
- 3.3 Bulk $\delta^{13}C$ measurements
- 3.4 Compound specific $\delta^{13}C$ measurements
- 3.5 Implications for the Eocene climate

5 Conclusion

Appendices
- A1 Scheme of the experimental set-up
- A2 Time series of pCO_2 and $\delta^{13}C$
- A3 Growth rates versus presence of algae
- A4 Differences between old and new material
- A5 Biological synthesis of lipid compounds

References

Acknowledgements

Climatic conditions governing extensive *Azolla* blooms during the Middle Eocene

Sediments from the Integrated Ocean drilling program expedition 302 contain high concentrations of intact remains of *Azolla* megaspores and microspore massulea, indicating that this free-floating aquatic fern grew and reproduced in situ in the Eocene Arctic Ocean. Today, *Azolla* inhabits fresh water bodies (the salinity tolerance of *Azolla* is 5), suggesting that the Arctic surface waters should have been fresh during the Eocene *Azolla* interval. Available proxy data and modeling results suggest that a reduced latitudinal temperature gradient prevailed during the interval. Furthermore, humidity was higher around the Eocene Arctic basin and the hydrological cycle was intensified during the Eocene. Here a compound specific hydrogen isotope signal for Eocene Central Arctic Ocean precipitation is presented for the first time. The results show isotopically heavy δD values for the Eocene Arctic precipitation (approximately -134‰) compared to todays (approximately -230‰). The heavy isotope signal of the Eocene Arctic precipitation is a consequence of reduced rainout over the equator-to-pole transect (as a consequence of the reduced latitudinal temperature gradient) and increased high latitude rainfall. Freshening of the Eocene Arctic surface waters can be reconstructed by calculating the degree of mixing between the surface water and the deeper saline waters. By comparing the δD value of the Eocene Arctic precipitation (-134‰) with the δD value of the Eocene Arctic surface waters, based on the δD signal of *Azolla* specific biomarkers (ranging between -116‰ and -133‰), and the δD value of modern Arctic surface waters (-8‰), mixing of the sea surface and deeper saline waters seems to be much reduced during the *Azolla* event. A quantification of the degree of mixing suggests that surface/deep water mixing during the Eocene was utmost 14.3%, resulting in a sea surface water salinity of only 0-4.8. The warmer Arctic SSTs and the freshening of the surface waters in the Early/Middle Eocene Arctic basin, confirms the prevalence of an environment where *Azolla* could have grown.

1. Introduction

In 2004 an expedition from the Integrated Ocean Drilling Program was challenged by drilling cores at the northern most location on Earth, only 250 km from the North Pole (87°52'N, 136°10'E), on the Lomonosov ridge. This expedition, leg 302, was successful in recovering sediments of Eocene age. The Eocene sediments consisted of alternating fine dark-grey clay layers and light-grey clay layers (Brinkhuis *et al*, 2006). Interestingly, the light-grey clay layers contained high concentrations of intact remains of *Azolla* megaspores and microspore massulae, indicating that this species grew and reproduced in situ in the Eocene Arctic Ocean (Brinkhuis *et al*, 2006). In the modern world, the free-floating aquatic fern *Azolla* inhabits warm temperate to tropical fresh water bodies, and can only tolerate salinities of utmost 5 (van Kempen *et al.*, in press). The occurrence of *Azolla* remains in the Eocene Arctic basin and the present habitat preferences of *Azolla*, suggests that a warmer and less saline environment could have prevailed in the Early/Middle Eocene Arctic surface waters.

The *Azolla* interval has been dated to Early/Middle Eocene age, from ~49.3 to ~48.1 Ma (Speelman *et al*, 2009a). During this interval, climatic conditions were substantially different than todays, with overall higher sea surface and air temperatures (amongst others Bijl *et al*, 2009; Brinkhuis *et al*, 2006; Pearson *et al*, 2007; Greenwood and Wing, 1995; Hollis *et al*, 2009) and enhanced greenhouse conditions, characterized by elevated CO_2 concentrations, with estimates ranging between 400-3000 ppm (Pearson and Palmer, 2000). In recent years numerous studies focused on reconstructing the

Eocene climate, as their improved insight in past climatic systems may be helpful in calibrating climate models. An overview of the available data on sea surface temperatures for the Early/Middle Eocene is summarized in figure 1 (adapted from Bijl *et al*, 2009). A comparison of sea surface temperature estimates from the Early/Middle Eocene (the orange line) and modern sea surface temperatures (the black line), suggests that overall absolute temperatures were considerably higher during the Eocene. And more importantly, the latitudinal temperature gradient appears to be more reduced 50 Ma than at present. During the Early/Middle Eocene, tropical sea surface temperatures were only slightly higher than today's, with average SSTs above 30°C (based on $\delta^{18}O$ of high quality samples of the Tanzanian coast, Pearson *et al*, 2007. Figure 1[g]). Sea surface temperatures at higher latitudes, on the other hand, show a larger difference with today's SSTs. High resolution sea surface temperature records of the Southern Pacific, based on a TEX_{86} SST record from the southwest Pacific Ocean [paleolatitude ~65° S] (Bijl *et al*, 2009) and based on a multi proxy record from New Zealand [paleolatitude ~55° S] (Hollis *et al*, 2009) both suggest temperatures of 25-30°C at high Southern latitudes (figure 1 [b] and [d] respectively). Furthermore, SST reconstructions from mid-to-high Northern latitudes suggest a similar trend on the Northern hemisphere (Sluijs *et al*, 2007; Brinkhuis *et al*, 2006, figure 1 [j,k] and [p] respectively). Brinkhuis *et al* (2006) suggests that SSTs for the central Arctic basin were 9-12°C. The prevalence of a reduced equator-to-pole temperature gradient is not limited to the oceanic realm, given that mean annual air temperature reconstructions illustrate that temperatures over the continents during the Eocene differed from the present. Data based on Early/Middle Eocene fossil leaves suggests that winter temperatures were elevated and that the latitudinal air temperature gradient over the continental interiors was more reduced compared to today's (Greenwood and Wing, 2005).

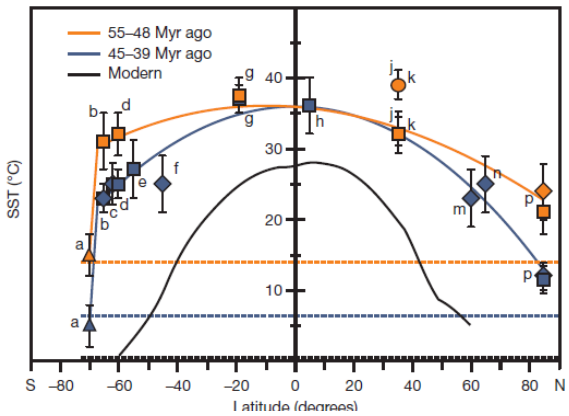

Figure 1. Latitudinal SST gradients of the Early/Middle Eocene (orange line) and modern (black line) (adapted from Bijl et al, 2009).

The warmer climate and the lower latitudinal temperature gradient during the Eocene has affected the hydrological cycle (Pagani *et al*, 2006; Speelman *et al*, 2010). Paleontological research on the *Azolla* interval has revealed that humidity levels fluctuated throughout this episode (Barke *et al,* in press), and was high around the Arctic basin (Greenwood *et al,* 2010). Using isotopic studies on fossilized *Metasequoia* on the Axel Heiberg Island (along the edge of the Arctic basin), humidity levels during the Eocene could be quantified to twice the modern amount (Jahren and Stenberg, 2003). Furthermore the Eocene Arctic precipitation was isotopically heavier than today's (Jahren *et al*, 2009; Speelman *et al,* 2010).

There is still much debate whether a reduced equator-to-pole temperature gradient could have prevailed during the Eocene (e.g. Huber and Sloan, 2000; Huber and Caballero, 2003). Ocean circulation models have not yet been able to regenerate a reduced latitudinal temperature gradient consistent with proxy SST results (e.g. Hollis *et al*, 2009). Though new modeling results by Speelman *et al* (2010) show that a modeled reduced equator-to-pole temperature gradient is consistent with available hydrogen isotope (δD) values for Early Middle Eocene precipitation (amongst others Jahren *et al*, 2009; Sessions *et al*, 1999). Here we record, for the first time, whether these modeling results can be applied to the central Arctic Eocene Ocean. This will be achieved by combining a TEX_{86} based sea surface temperature reconstruction with a δD precipitation reconstruction from the Lomonosov ridge. Additionally, the reconstructed hydrogen isotopic values for the Eocene Arctic precipitation will be compared with δD values for the Eocene Arctic surface waters (Speelman, personal communication), to evaluate whether a freshwater environment could have prevailed during the Early/Middle Eocene, supporting the growth of *Azolla*.

2. Background information

2.1 Geochemically reconstructing Sea surface temperatures

Scientists have attempted to reconstruct sea surface temperatures for a long time, since it is a major constituent of Earth's climate system. Different methods have been established over the years, based on a variety of principles. Where reconstructions of continental air temperatures are mostly based on pollen, micro- and megaspore assemblages, congregations of planktonic saltwater species (e.g. foraminifera) form the basis of paleontological sea surface temperature (SST) estimates. Since reconstruction methods are affected by numerous uncertainties and assumptions, the use of multiple independent proxies is preferred. In addition to the paleontological methods for temperature reconstructions, independent geochemical proxies have been developed. Examples of these proxies are SST reconstructions based on the $\delta^{18}O$ composition and on the Mg/Ca ratio of calceous organisms, on the composition of long-chain unsaturated ketones from coccolithiphorids ($U^{k`}_{37}$, Müller *et al*, 1998) and on the number of cyclopentane rings in Archaeal membrane lipids, the TEX_{86} proxy.

TEX_{86} (TetraEther indeX of tetraethers consisting of 86 carbon atoms) is an independent sea surface temperature proxy based on the relative distribution of glycerol dialkyl glycerol tetraethers (GDGTs) with one or more cyclopentane rings (Schouten *et al*, 2002). These membrane lipids are present in Archaea and are used to adapt the flexibility of the Archaeal membrane to varying environmental temperatures, where the number of cyclopentane rings increases when the surrounding temperature rises (Schouten *et al*, 2002). The temperature signal in the GDDT's reflects the temperature of the upper layers of the oceans, and is transported downwards by both passive transport (in the form of POM), and by active transport (by ingesting) (Huquet *et al*, 2006). During both transport pathways, the composition of the membranes and consequently the TEX_{86} signal remains unchanged. Therefore, the sedimentary TEX_{86} signal is thought to ultimately reflect the original temperature conditions in the surface waters. In nature, GDGTs occur in a range of structures, which can be separated into three groups; the isoprenoid GDGTs [I-V], crenarchaeol (specific for crenarcheota) [VI] and branched GDGTs [VII-IX] (structures of all GDGT species are presented in the supplementary information). Marine environments, the setting of interest for the sea surface temperature reconstruction, contain Archaeae that produce crenarchaeol (~50%) and

isoprenoid GDGTs [II-IV] (~16%). In terrestrial sediments, on the other hand, membrane lipids from all three groups can be found (Weijers *et al*, 2006). Interestingly, only terrestrial Archaeae produce branched GDGTs. When using the TEX_{86} proxy for a SST reconstruction, one must discriminate between the aquatic or terrestrial origin of the GDGTs. For this purpose, the BIT-index (Branched and Isoprenoid Tetraether-index) can be applied. The BIT-index is a proxy for the amount of terrestrial organic matter in sediments, based on the relative abundance of branched GDGTs (only produced in situ by terrestrial Archaea) and crenarchaeol (derived from both marine and lacustrine settings) (Hopmans *et al*, 2004).

When applying TEX_{86} measurements for sea surface reconstructions in this thesis, the BIT-index is determined as well, to assess whether the sedimentary TEX_{86} signal truly represents surface water temperatures.

2.2 Geochemically reconstructing Eocene Arctic precipitation

The isotopic composition of environmental water (H_2O) is incorporated in both hydrogen and oxygen isotopes (δD [D/H] and $\delta^{18}O$ [$^{16}O/^{18}O$], respectively). Both isotope ratios change according to a linear trend, following the meteoric water line (Craig, 1961), but the absolute δD and $\delta^{18}O$ values might differ in time and space as the isotopic composition of precipitation is affected by (1) the original isotopic composition of its source waters, (2) the so called 'rain-out effect' (the preferential loss of heavier isotopes during transport) and (3) air temperature at the site of cloud collection (Craig and Gordon, 1965; Merlivat and Jouzel, 1979). Originally, δD and $\delta^{18}O$ values of precipitation were measured by looking at isotope ratios of plant cellulose (Sternberg, 1988). However, isotopic fractionation within plants (during water uptake, evapotranspiration and cellulose synthesis) makes the interpretation of the hydrogen isotopic signature of the (meteoric) source water complicated. For this reason plant components which incorporate hydrogen with minor metabolic effects (such as *n*-alkyl lipids, *n*-alkenols, and sterols) are currently commonly used for meteoric hydrogen reconstructions (Sternberg, 1988; Sauer *et al*, 2001).

In order to reconstruct the δD signature of the Early/Middle Eocene Central Arctic precipitation, hydrogen isotopes on long chain *n*-alkanes were analyzed. *n*-Alkanes with chain lengths of 23 to 35 carbon atoms (*n*-C_{23} to *n*-$_{C35}$) and an odd-over-even predominance are typically derived from the leaf waxes of higher plants. Furthermore, plants are suggested to primary incorporate the hydrogen composition of the local precipitation (Sauer *et al*, 2001), making the long chain *n*-alkanes suitable for the purposes of this thesis.

The preferential use of hydrogen over deuterium isotopes in biological and physical processes makes the original δD value of the meteoric water heavier compared to the δD signal of the lipids. The isotopic fractionation between δD_{lipid} and δD_{water} ($\varepsilon_{(n\text{-alkane} - water)}$) can be determined by comparing the hydrogen isotopic composition of lipids from cultured plants with the isotopic composition of the source water.

In this thesis three fractionation values (ε = -117‰, ε = -105‰ and ε = -62‰) and are used, the first adapted from Chikaraishi & Naraoka (2003) and the latter two from Yang *et al* (2009), respectively. The fractionation factor determined by Chikaraishi & Naraoka (2003) is presently the most applicable value for $\varepsilon_{(n\text{-alkane} - water)}$ (e.g. Jahren *et al*, 2009). This fractionation factor is based on an average ε-value for modern C_3 plants, though recent publications have suggested that internal fractionation is

species specific (e.g. Chikaraishi *et al*, 2004), due to different kinetic isotope effects of key biochemical reactions of each plant (*cf* Chikaraishi *et al*, 2004) and interspecies differences in water budgets (Liu *et al*, 2006). Yang *et al* (2009) have focused their research solely on *Metasequoia* species. *Metasequoia* is suggested to be the dominant species in the deciduous conifer forest found along the Eocene Arctic basin (Jahren *et al*, 2009). Greenhouse experiments by Yang *et al* (2009) have revealed that $\varepsilon_{(\text{n-alkane} - \text{water})}$ for *Metasequoia* was approximately -105‰. Interestingly, they have also grown *Metasequoia* under a continues light regime, since the Arctic regions have a steady low intensity light supply during the growing season. These experiments suggest an $\varepsilon_{(\text{n-alkane} - \text{water})}$ twice as small as under a normal light regime (ε= -62‰), as an effect of enhanced transpiration during the prolonged illumination regime, resulting in deuterium enrichment of the leaf water.

3. Materials and methods

3.1 Sample material

3.1.1 Sea surface temperature reconstruction: TEX_{86}

For the reconstruction of sea surface temperatures of the Arctic basin and the latitudinal temperature gradient, samples from various locations around the Arctic basin and on lower latitudes are used for the TEX_{86} reconstruction. All samples are dated for Early/Middle Eocene age, coinciding with the *Azolla* interval. The sampling locations are shown in figure 2 on a latitudinal scale and details on the locations are listed in table 1.

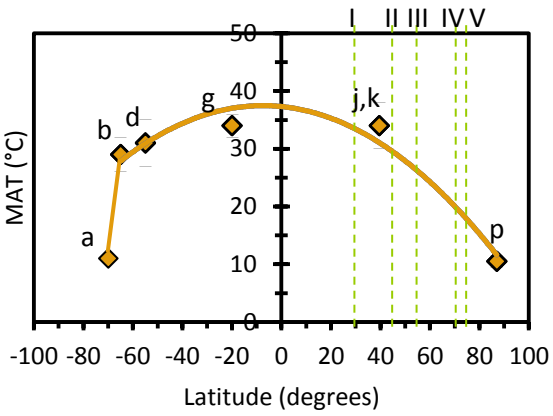

Figure 2. Sample locations on a latitudinal scale. Roman numbers correspond with table 1.

Table 1. Detailed description of the sampling locations

	Sample	Location	Latitude/longitude		Waterdepth (m)	Reference
V	IODP leg 151 site 0913B cores 46-49	Greenland Sea	75°29'N	6°57'W	3318	IODP database
IV	Sandpiper	Beaufort sea	70°N	148°W	Unknown	Unpublished data
III	Danish Outcrops	North Sea, Denmark	55°N	10°W	Well below wave base	Heilmann-Clausen *et al*, 1985
II	ODP leg 171 site 1052	Florida Atlantic margin	30°3'N	76°21'W	1982	IODP database
I	Possagno Outcrop	Northern Italy	45°51'N	11°52'E	Unknown	Agnini *et al*, 2006

Hydrogen cycle reconstruction

The samples used for the hydrogen cycle (δD precipitation) reconstruction were recovered during the IODP 302 ACEX expedition, at the Lomonosov ridge (87°52'N, 136°10'E, at a water depth of 1288 m. In this study, sediments from lithological Unit 2 (core M0004A-11 x 297.31 – 302.63 mbsf) were used. These sediments are dominated by very dark clay mud-bearing biosilicious ooze, with pale-grey laminations (Speelman *et al*, 2009a). Samples were selected based on the organic carbon content, as determined by Speelman *et al* (2009a).

3.2 Methods

3.2.1 TEX_{86} and BIT analyses

The sediment samples used for the TEX_{86} measurements (listed in table 1) were freeze-dried, powdered and subsequently extracted with an Accelerated Solvent Extractor (Dionex ASE 200), using a dichloromethane (DCM): Methanol (MeOH) (9:1, v/v) mixture. To separate the compounds of interest (GDGTs for the TEX_{86} sea surface temperature determination), the total extracts were separated with Al_2O_3 column chromatography, using hexane:DCM (9:1) and DCM:Methanol (MeOH) (1:1) mixtures to yield the apolar [F1] and polar [F2] eluents respectively. The polar fraction, containing the GDGTs, was subsequently dissolved in an isopropane:hexane (99:1, v/v) mixture and filtered using a PTFE filter. The polar fractions were analyzed for TEX_{86} using high-performance liquid chromatography/mass spectrometry (HPLC/MS) at NIOZ (Texel, Netherlands) (following Schouten *et al*, 2007). The integrated results were converted to sea surface temperatures using both the calibration of Schouten *et al* (2002) (eq 1) and Kim *et al* (2008) (eq 2).

$T = (TEX_{86} - 0.28) / 0.015$ ($r^2 = 0.92$) (Equation 1)

$T = -10.78 + 56.2 * TEX_{86}$ ($r^2 = 0.935$) (Equation 2)

In addition to the TEX_{86} calibrations for saline water systems (eq 1 and eq 2), a TEX_{86} calibration for fresh water systems was used. This was performed as the input of freshwater into the Eocene Arctic basin was possibly high (Brinkhuis *et al*, 2006; Speelman *et al*, 2009a). As a result a fresh water lens might have developed during the *Azolla* interval. Lacustrine environments contain crenarchaeota with a biological mechanism to adapt their membrane to environmental conditions similar as their marine counterparts (Powers *et al*, 2004). The lacustrine TEX_{86} calibration used in this paper is adapted from Blaga *et al* (2009) and is based on 48 core top lake sediment samples (eq 3).

$T = (TEX_{86} - 0.19) / 0.018$ ($r^2 = 0.76$) (Equation 3)

3.2.2 δD measurements

Freeze-dried and powdered samples from IODP leg 302 were extracted with an Accelerated Solvent extractor (Dionex ASE 200), using a dichloromethane (DCM): Methanol (MeOH) (9:1, v/v) mixture. Functional compounds within the total extracts were separated by silicate chromatography, using hexane [F1], DCM [F2] and MeOH [F3] as subsequent eluents. Since all sediment samples contained elemental sulfur, the different fractions were desulphurized using activated copper (the copper was activated using a 0,1M HCl solution). The apolar [F1] fraction was purified by urea adduction (with [A1] for the adductable normal and isoalkanes and [A2] for the non-adduct), after which A1 was further purified by $AgNO_2$ chromatography (using *n*-hexane for the saturated *n*-alkane compounds [A1] and DCM for the rest). The saturated *n*-alkanes [A1] and hopanes [A2] were indentified using gas chromatography/mass spectrometry (GC/MS) spectra (Thermo Trace GC Ultra, Thermo Fisher Scientific Inc.). Samples were on-column injected at 70°C, on a CP-sil 5CB fused silica column (30 m x 0.32 mm i.d., film thickness 0.1 µm) with helium as carrier gas set at constant pressure (100 KPa). The oven was programmed to 130°C at 20°C min^{-1} and then to 320°C at 4°C min^{-1}, followed by an isothermal hold for 20 min. Subsequently, compound specific δD values were determined using isotope ratio monitoring gas chromatography-mass spectrometry (GC-IRMS), using a ThermoFinnigan Delta-Plus XP mass spectrometer. A similar column and over program was used as for the GC/MS measurements, though injection was performed using an autosampler (Gerstel MPS 2 twister) with a 10 ml syringe with 70mm needle length. The compounds were converted using a high temperature conversion reactor (1400 °C). During all sample and standard measurements, pulses of reference gas were discharged into the IRMS for 20 seconds as a reference gas for the calculation of relative δD values and drift correction. Co-injected squalane, with an offline determined isotopic composition was used as internal standard . Hydrogen isotopic compositions are reported against Vienna standard mean ocean water (VSMOW) and are based on duplicate analyzes, with a precision of 0,5-5‰. Furthermore, all hydrogen isotope values discussed in this thesis, exceeded a minimal level of 500 mV. The mixed [F2] fraction contained fatty acid methyl esters (FAME). The polar [F3] fraction was methylated with BF_3/MeOH at 60°C for 10 min and silylated with BSTFA in pyridine at 60°C for 20 min (to convert the alcohols into the corresponding TMS-ethers). The F3 fraction contained the characteristic *Azolla* biomarkers (C_{30}-C_{36} 1,ω20 diols) (Speelman *et al*, 2009b). Both the F2 and F3 fractions were identified using the GC/MS spectra and analyzed for hydrogen isotope values using GC-IRMS, following the same methods as described for the A1 and A2 fractions.

Before separation with silicate chromatography, the largest three extracts were desulphurized using a Raney Nickel catalyst to break any diagenetic sulfur bonds, following Sinninghe Damsté *et al* (1988). As a result the amount of saturated *n*-alkane compounds was increased for improved analysis. After this treatment the samples were handled and purified with the same methods as all other samples.

4 Results and discussion

4.1 Temperatures in the Arctic basin

Sediment samples from various locations around the Eocene Arctic Basin have shed more light on the sea surface temperatures (SSTs) at high Northern latitudes (figure 3). For all locations, the resulting SSTs using the TEX_{86} calibration by Kim *et al* (2008) are preferred to the resulting SSTs using the TEX_{86} calibration by Schouten *et al* (2002), since the calibration by Kim *et al* (2008) is based on more core-top sediment samples and shows a higher correlation between the sediment samples and the mean

annual temperature. For the sea surface temperature reconstruction using both calibrations and variations between them, see appendix A2.

The sea surface temperature record based on the calibration for lacustrine environments by Blaga *et al* (2009) shows similar SST values as the calibration by Kim *et al* (2008) for marine systems (appendix A2). This suggests that Eocene sea surface temperature reconstructions based on fresh water Archaea fall in the same range as the marine Archaea based SSTs.

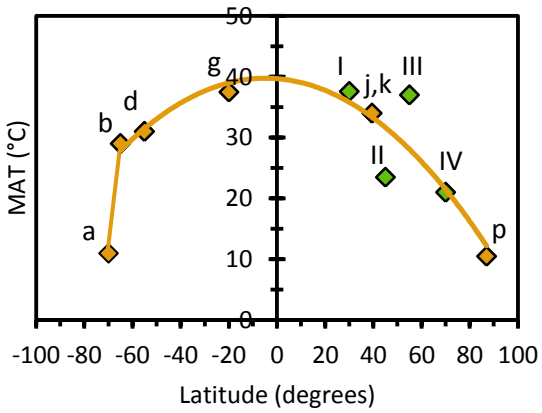

Figure 3. Latitudinal temperature gradient of Eocene Sea surface temperatures. The orange diamonds represent data from literature studies, the green diamonds represent new TEX86 measurements discussed in this paper.

Temperatures around Alaska [Beaufort Sea] (figure 3 IV) seem slightly higher than those at the North Pole itself [Lomonosov ridge], though they fit well with the lowered latitudinal temperature gradient during the middle Eocene. The increase of surface water temperature around Alaska against the North Pole could be explained by the setting of both locations. The core from the Beaufort Sea is drilled further south and close to the coastline, suggesting a near coastal deposition. This is validated by the occurrence of pebbles in this core. The core from the Lomonosov ridge, on the other hand, is drilled on a high rim in the center of the Arctic Ocean, where coastal influences were absent.

Unfortunately samples from IODP leg 151 site 0913B cores 46-49, did not contain sufficient Archaeael membrane lipids (GDGTs), for a significant TEX_{86} based SST reconstruction. At the time of drilling, the depth of the basin was over 3 km. Assuming the basin bathymetry has not changed much for the last 50 Million years (ref), the deficient amount of GDGTs could be explained by insufficient particle settling as the basin was too deep for adequate particle settling.

Furthermore, TEX_{86} measurements from samples of the Danish coast show exceptionally high sea surface temperature values (~37°C, figure 3 III). Sediment samples from the Danish coast are gathered from outcrop material and erosion could have affected the preservation of the GDGTs in the sediments. Soil Archaea could have influenced the pristine marine TEX_{86} signal, although this is not reflected in the low BIT-index (0.06).

4.2 Latitudinal temperature gradient

In addition to samples from mid-to-high northern latitudes, sediment samples from (sub)tropical regions have been analyzed for reconstructing SSTs. Samples from the Florida margin (figure 3 I), show that Eocene SSTs from low latitudes follow the reduced meridional temperature gradient.

Furthermore, SSTs from the Florida margin fall in the range of other sea surface temperatures estimates for subtropical waters (e.g. Pearson *et al*, 2007).

As with the samples from the Danish outcrops, samples from the Northern Italian coast [Possagno] (figure 3 II) do not fall in line with the latitudinal temperature gradient. Samples from Possagno displayed a high BIT-index (between 0.54 and 0.88), suggesting that the input of terrestrial material was substantial. As a result, the fluvially transported crenarcheotal membrane lipids (GDGT VI) have biased the pristine sea surface temperature signal from these sediments (Weijers *et al*, 2006). These samples can thus not be used for TEX86 reconstruction.

4.3 Hydrological cycle reconstruction

All sediment samples used for the δD precipitation reconstruction contain a range of long-chain (C_{23}-C_{35}) *n*-alkanes with a strong odd-over-even predominance (figure 4). Within this series of n-alkanes, *n*-C_{29} has the highest abundance, as is consistent with mass-spectrometry findings of Eocene Arctic vegetation (Jahren *et al*, 2009). Additionally, the prevalence of C_{29}-alkanes reflects the whole leaf signature of *Metasequoia* spp, the dominant species in the deciduous conifer forest found along the Eocene Arctic basin (Jahren *et al*, 2009). *n*-Alkanes with shorter chain lengths (<C_{20}), typical for algal and (photosynthetic) bacterial input (Pagani *et al*, 2006), are absent in the samples, implying that any microbial influence on the specific hydrogen isotopic signal can be neglected. The finding of only long chain odd-over-even (C_{23}-C_{35}) *n*-alkanes with a C_{29}-alkane dominance suggest that the δD composition of the extracted *n*-alkanes from the ACEX sediments, reflect the pristine hydrogen isotopic signal of the Eocene Arctic precipitation.

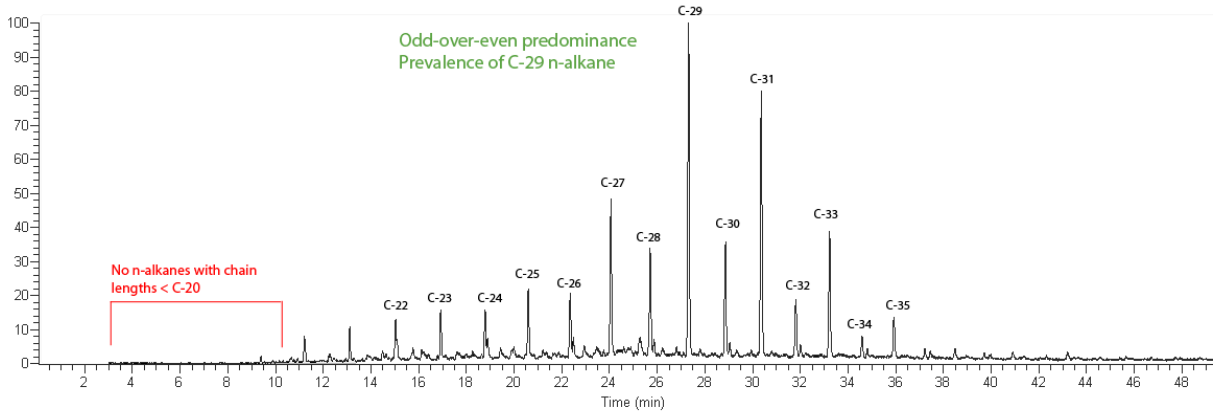

Figure 4. GC-MS chromatogram of n-alkane [A1] fraction.

GC-IRMS results are summarized in table 2. There is a large variation in $\delta D_{n\text{-alkane}}$ values between *n* within one sample. A natural variety in the hydrogen isotopic values is common amongst hydrocarbons of different chain lengths (Sessions *et al*, 1999; Chikaraishi and Naraoka, 2003; Sachse *et al*, 2006, Zhou *et al* (2010), with a slight δD enrichment towards longer *n*-alkanes, and heavier δD values for *n*-alkanes with even chain lengths (compared to *n*-alkanes with an odd number of carbon atoms). They reasoned that differences in δD values between even and odd chain length could be explained by different biosynthetic pathways (Zhou *et al*, 2010), and where biosynthetic pathways

are similar, the variations in δD may be associated with differences in the isotopic composition of the original biosynthetic precursor or of the added hydrogen (Sessions *et al*, 1999).

Table 2 Hydrogen isotopic values of two samples

Sample/compound	δD_{lipid} (‰)*	δD_{water} (‰)*[A]	δD_{water} (‰)*[B]	δD_{water} (‰)*[C]
ACEX 11/ 2W/ 121-122				
n-C27 alkane	-210	-93	**-105**	-148
n-C29 alkane	-239	-122	**-134**	-177
ACEX 11/4W/25-29				
n-C26 alkane	-247	-130	**-142**	-185
n-C28 alkane	-250	-133	**-145**	-188
n-C29 alkane	-223	-106	**-119**	-161

** measured against SMOW*

A ε based on Chikaraishi and Naraoka (2003)

B ε based on Yang et al (2009)

C ε based on Yang et al (2009) – continues light regime

The original hydrogen isotopic composition of the source water is altered during lipid synthesis (section 2.2), making the $\delta D_{n\text{-alkane}}$ signal more enriched. The hydrogen isotope signal of the precipitation (δD_{water}) is calculated from the measured δD value for the lipids ($\delta D_{n\text{-alkane}}$) using a fractionation factor ($\varepsilon_{(n\text{-alkane} - water)}$). Here three fractionation values (ε = -117‰, ε = -105‰ and ε = -62‰) and are used, the first adapted from Chikaraishi & Naraoka (2003) and the latter two from Yang *et al* (2009), respectively (section 2.2).

For all three fractionation factors, the calculated hydrogen isotope values for Eocene Arctic environmental water (δD_{water}) suggest that the precipitation during this period was isotopically enriched compared to modern Arctic precipitation [-230 ‰] (GNIP database) (table 2). The enrichment in δD_{water} during the Eocene could be explained by an enhanced hydrological cycle. When the latitudinal temperature gradient is more reduced, rainfall along the equator-to-pole transect is more decreased (Speelman *et al*, 2010). As a consequence, the hydrogen isotope value of the atmospheric water vapor is not affected by the rain-out effect along the equator-to-pole transect. The resulting precipitation around the Arctic will be isotopically heavier (Craig and Cordon, 1965), as is consistent with the δD signal of the Eocene precipitation discussed in this thesis.

Furthermore, the hydrogen isotopic composition of the Eocene Arctic precipitation, as measured using δD signal from *n*-alkanes, combined with the Eocene sea surface temperature at this location, are in line with modeling results by Speelman *et al* (2010), figure 5. They have modeled the isotopic composition of precipitation and vegetation during the Eocene. Climatic conditions during the Eocene differed quite from today's, with overall higher temperatures and enhanced carbon dioxide conditions, influencing the growth of vegetation and in turn the isotopic fractionation of hydrogen isotopes during uptake. The results discussed in this thesis fall within the δD range for the Eocene suggested by Speelman *et al* (2010).

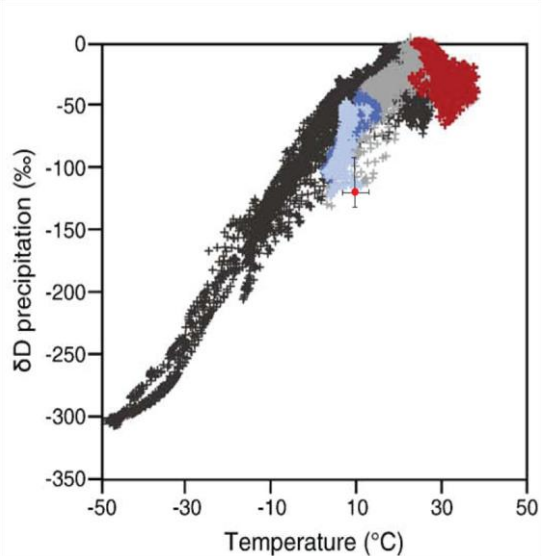

Figure 5. Modeling results by Speelman et al (2010). Black dots represent the δD signal of modern precipitaton and the light blue dots the Eocene δD precipitaton at the Arctic. The red dot represents the proxy-inferred precipitation dD signal as presented in this thesis.

4.4 Sea surface mixing and salinity

Azolla specific compounds (C_{30}-C_{36} 1,ω20 diols) (Speelman *et al*, 2009a) reflect the isotopic composition of the surrounding surface ocean water, since surface water is the main source for hydrogen in *Azolla*. Measurements on the hydrogen isotopic composition of the *Azolla* biomarker suggest that the δD signature of the Arctic surface waters was in the range of -116 to - 133‰. When there is no ice on Earth, as during the warm Eocene, the δD signature of the oceanic surface waters is generally lighter [-8‰]. The isotopic signature of the surface waters is dependent on the amount of mixing between generally isotopic heavy saline deeper waters and isotopic lighter precipitation. The highly δD depleted Arctic surface waters during the *Azolla* interval imply that mixing between the surface and deeper waters during the interval has been minimal. By completing the following mass balances, a quantification of the amount of mixing can be added.

$$\delta D_{\text{Eocene surface waters}} = a * \delta D_{\text{precipitation}} + (1-a) * \delta D_{\text{Arctic ocean waters}} \quad \text{(Equation 4)}$$

$$S_{\text{Eocene surface waters}} = a * S_{\text{precipitation}} + (1-a) * S_{\text{Arctic ocean waters}} \quad \text{(Equation 5)}$$

With equation 4 the fractions of Arctic Ocean surface water that originated from precipitation (*a)* and deeper ocean waters (1-*a*) can be calculated, based on the isotopic composition of both. Equation 5 makes use of the determined value of *a* and (1-*a*) to calculate the salinity of the surface water assuming that precipitation only consists of freshwater (0 psu) and that the average salinity of ocean water (without ice) is about 34 psu. By completing both equations, mixing between the Arctic surface and deeper waters during the Eocene can be determined and was max 14.3% for the Eocene (figure 6) confirming freshening of the Eocene Arctic surface waters and the realization of an environment where *Azolla* is able to grow. In contrast to the low saline conditions in the surface waters, the salinity of the deeper water was higher, ranging between 15-21 (Waddell and Moore, 2008). As a result of the low surface water mixing a strong halocline prevailed at the Eocene Arctic Ocean (Waddell and Moore, 2008). In combination with the highly laminated Eocene sediments found at the central Arctic (Brinkhuis *et al*, 2006) suggests that the basin was highly stratified during the

Early/Middle Eocene. The stratification of the Arctic waters is furthermore illustrated by increased organic carbon accumulation rates (e.g. Knies *et al*, 2008) and the enrichment of trace metal elements as Co, Cu, Fe, Mo, V and Zn (e.g. März *et al,* 2010).

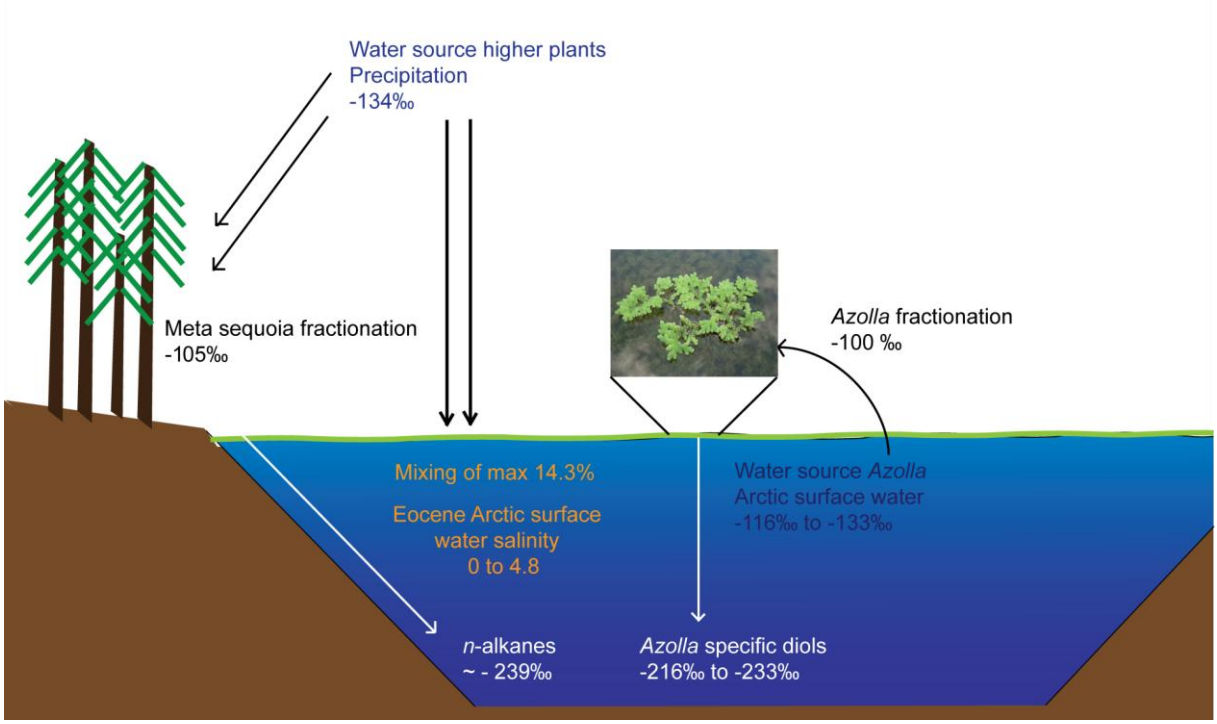

Figure 6. Representation of sea surface and deep water mixing and salinity during the Azolla interval, based on proxy data.

5. Conclusion

The research presented in this thesis confirms that temperatures around the Arctic have been warmer during the Eocene and that the latitudinal temperature gradient was more reduced 50 Ma, compared to today's. The effect of the reduced latitudinal temperature gradient on the hydrological cycle is revealed with a reconstruction of the hydrogen isotopic signal of the Eocene Arctic precipitation. Precipitation at high Northern latitudes (78°N) was heavier during the Eocene than at present (δD_{eocene} = -134‰; δD_{modern} = -230‰), suggesting an intensification of the hydrological cycle/ The intensified hydrological cycle is associated with less rain-out over the equator-to-pole transect and more and isotopically heavier precipitation at higher latitudes. The proxy-inferred isotopic signal of the Eocene precipitation is in line with modeling results by Speelman *et al* (2010). The increased precipitation facilitated the prevalence of a fresh water layer (salinity ranging between 0-4.8) on top of the deeper saline Arctic waters. As a consequence, surface-deep water mixing was minimal (utmost 14.3%), resulting in a strong halocline in the basin. The strong halocline and the laminated sediments from IODP leg 302, suggest that the Eocene Arctic basin was highly stratified. Overall, the surface waters of the Early/Middle Eocene Central Arctic basin were warm and especially fresh, providing an environment where *Azolla* could have grown.

Appendix

A 1. GDGT structures, TEX_{86} algorithm and BIT-index

GDGTs are generally separated into three groups, the isoprenoid GDGTs [I-V], crenarchaeol (specific for crenarcheota) [VI] and branched GDGTs [VII-IX]. Structures of these compounds are drawn in figure A1 (adapted from Weijers *et al*, 2006).

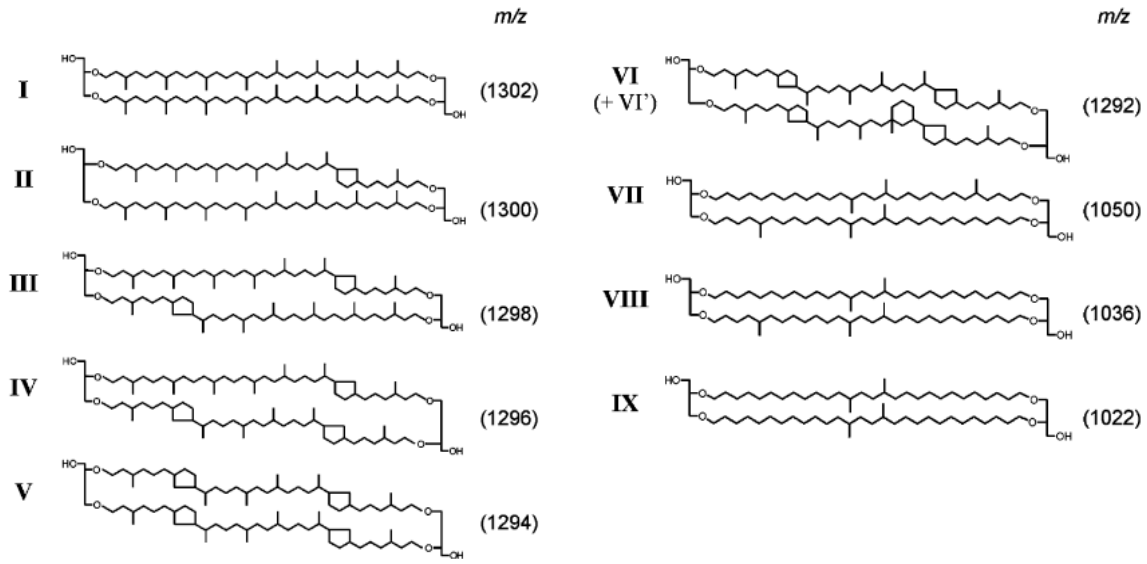

Figure A1. Structures of GDGTs [I to IX], with their characteristic m/z values.

For the TEX_{86} temperature proxy, the ratio between isoprenoid GDGTs [I-V] and crenarchaeol [VI] is determined using the algorithm in equation A1. In addition, the BIT-index, used to determine the influence of terrestrial GDGTs on the pristine marine TEX_{86} derived SST signal, is calculated by comparing crenarchaeol [VI] and branched GDGTs [VII-IX] (eq A2).

$$TEX_{86} = \frac{([IV]+[V]+[VI])}{([III]+[IV]+[V]+[VI])}$$ (Equation A1) (Schouten *et al*, 2002)

$$BIT = \frac{([IX]+[VIII]+[VII])}{([IX]+[VIII]+[VII]+[VI])}$$ (Equation A2) (Hopmans *et al*, 2004)

A 2. Comparing TEX_{86} calibrations

For the reconstruction of the sea surface temperatures (SST) both the calibrations of Schouten *et al* (2002) and Kim *et al* (2008) were used. Figure A2 presents the latitudinal SST temperature gradients based on both calibrations. The calibration by Schouten *et al* (2002) seems to result in slightly decreased SST values at higher latitudes and increased SST values at mid-to-low latitudes (blue lines) in comparison to SST values using the Kim *et al* (2008) algorithm. This makes the calibration by Kim *et al* (2008) slightly more sensitive than the calibration by Schouten *et al* (2002), and preferable to use.

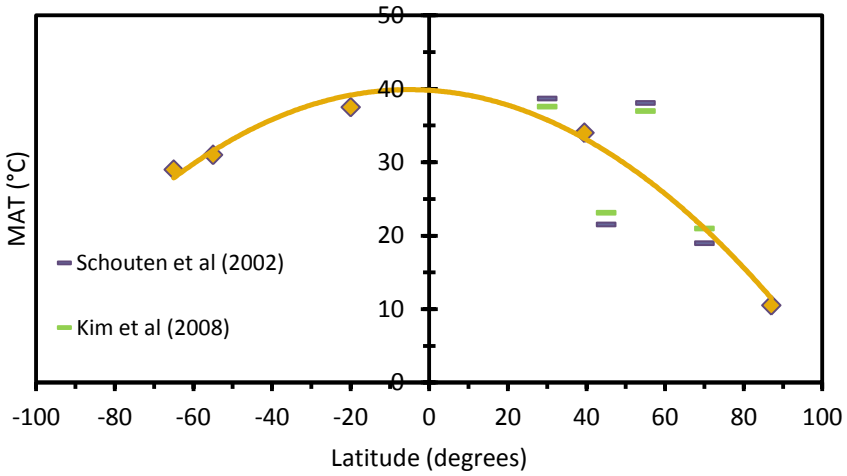

Figure A2. Latitudinal SST gradient using the Kim et al (2008) and Schouten et al (2002) calibration, represented by the green dots and blue diamond's respectively.The orange diamonds are adapted from literature studies.

Table A2 shows the resulting sea surface temperature of the Beafort Sea samples, using a marine TEX_{86} and lacustrine TEX_{86} calibration. Interestingly both calibrations result in a similar SST, suggesting that freshwater SSTs fall in the same range as the marine SST, for the Eocene Arctic Ocean.

Table A2. Comparison between marine TEX_{86} core top calibration by Kim et al (2008) and lacustrine TEX_{86} core top calibration by Blaga et al (2009).

Location		Sea surface temperature (°C) (Kim *et al*, 2008)	Sea surface temperature (°C) (Blaga *et al*, 2009)	Source
70°N	Beafort Sea, Alaska	21,0	20,8	Sandpiper

A 3. Other compound occurrence

In addition to the compounds of interest discussed in this paper (C_{23}-C_{35} *n*-alkanes and C_{30}-C_{36} 1,ω20 diols), many other organic components have been found and/or have been missed in the sediments. For example, long-chain unsaturated *n*-alkenones (derived from haptophytes and used by the U_k^{37} sea surface temperature proxy (Müller *et al,* 1998), have not been found in the Eocene Arctic sediments. This seems trivial, but previous research by Weller and Stein (2008) have made SST approximations of the Eocene Arctic based on this proxy, using the same sediments from the IODP leg 302. For this reason, this reference was not used in the latitudinal temperature gradient generated in figure 1. Among the interesting compounds that were present in the sediments are fatty acid methyl esthers (FAME). Under general circumstances, these fatty acids only found with the methyl group, after this is attached due to laboratory treatment (methylation). However the ACEX sediments recovered long chain (C_{16}-C_{32}) methylated fatty acids, suggesting an (so far) unknown process is involved. Since the δD values of the FAME's are in the range of the hydrogen isotopic signal of the *n*-alkanes (-223‰ to -251‰) they could be an interesting subject for further research.

References

Bijl, P.K., Schouten, S., Sluijs, A., Reichart, G.J., Zachos, J.C., Brinkhuis, H., 2009. Early palaeogene temperature evolution of the southwest Pacific Ocean. Nature 461, 776-779.

Blaga, C.I., Reichart, G.J., Heiri, O., Sinninghe Damsté, J.S., 2009. Tetrhether membrane lipid distributions in water-column particulate matter and sediments: a study of 47 European lakes along a north-south transect. Journal of Paleolimnology, 41, 523-540.

Brinkhuis, H., Schouten, S., Collinson, M.E., Sluijs, A., Sinninghe Damsté, J.S., Dickens, G.R., Huber, M., Cronin, T.M., Onodera, J., Takahashi, K., Bujak, J.P., Stein, R., van der Burgh, J., Eldrett, J.S., Harding, I.C., Lotter, A.F., Sangiorgi, F., van Konijnenburg-van Cittert, H., de Leeuw, J.W., Matthiessen, J., Backman, J., Moran, K.The Expedition 302 Scientists, 2006. Episodic fresh surface waters in the Eocene Arctic Ocean. Nature 441, 606–609.

Chikaraishi, Y., Naraoka, H., 2003. Compound-specific δD-δ^{13}C analyses of *n*-alkanes extracted from terrestrial and aquatic plants. Phytochemistry 63, 361-371.

Chikaraishi, Y., Naraoka, H., Poulson, S.R., 2004. Hydrogen and carbon isotope fractionations of lipid biosynthesis among terrestrial (C3, C4 and CAM) and aquatic plants. Phytochemistry, 65, 1369-1381.

Claudia Agnini, C., Muttoni, G., Kent, D.V., Rio, D., 2006. Eocene biostratigraphy and magnetic stratigraphy from Possagno, Italy: The calcareous nannofossil response to climate variability. EPSL 241, 815– 830.

Craig, H., 1961. Isotopic variations in meteoric waters. Science 133, 1702-1703.

Craig, H., Gordon, L.I., 1965. Deuterium and oxygen 18 variations in the ocean and the marine atmosphere, in Stable Isotopes in Oceanographic Studies and Paleotemperatures. Lab. di Geol. Nucl., Pisa, Italy, pp. 9–130.

Greenwood, D.R., Wing, S.L., 1995. Eocene continental climates and latitudinal temperature gradients. Geology 23, 1044-1048.

Greenwood, D.R., Basinger, J.F., Smith, R.Y., 2010. How wet was the Arctic Eocene rain forest? Estimates of precipitation from Paleogene Arctic macrofloras. Geology 38, 15-18.

Heilmann-Clausen, C., Nielsen, O.B., Gersner, F., 1985. Lithostratigraphy and depositional environments in the Upper Paleocene and Eocene of Denmark. *Bull. geol. Soc. Denmark,* vol. 33, pp. 287-323.

Hollis, C. J., Handley, L., Crouch, E.M., Morgans, H.E.G., Baker, J.A., Creech, J., Collins, K.S., Gibbs, S.J., Huber, M., Schouten, S., Zachos, J.C., Pancrost, R.D., 2009. Tropical sea temperatures in the high latitude South Pacific during the Eocene. Geology 37, 99–102.

Hopmans, E.C., Weijers, J.W.H., Schefuß, E., Herfort, L., Sinninghe Damsté, J.S., Schouten, S., 2004. A novel proxy for terrestrial organic matter in sediments based on branched and isoprenoid tetraether lipids. EPSL 224, 107– 116.

Huguet, C., Cartes, J.E., Sinninghe Damsté, J.S, Schouten, S., 2006. Marine crenarchaeotal membrane lipids in decapods: Implications for the TEX86 paleothermometer. Geochemistry Geophysics Geosystems ….??

IAEA/WMO, 2006. Global Network of Isotopes in Precipitation. The GNIP Database. 395 Accessible at: http://isohis.iaea.org

Jahren, A.H., Sternberg, L.S.L., 2003. Humidity estimate for the middle Eocene Arctic rain forest. Geology 31, 463-466.

Jahren A.H., Byrne, M.C.,Graham, H.V., Sternberg, L.S.L., Summons, R.E., 2009. The environmental water of the middle Eocene Arctic: Evidence from δD, $\delta^{18}O$ and $\delta^{13}C$ within specific compounds. Palaeogeogr., Palaeoclimatol., Palaeoecol. 271, 96-103.

Kim, J.H., Schouten, S., Hopmans, E.C., Donner,B., Sinninghe Damsté, J.S., 2008. Global sediment core-top calibration of the TEX86 paleothermometer in the ocean: Geochimica et Cosmochimica Acta 72, 1154–1173.

Knies, J., Mann, U., Popp, B.N., Stein, R., Brumsack, H-J., 2008. Surface water productivity and paleoceanographic implications in the Cenozoic Arctic Ocean. Paleoceanography, 23, PA1S16.

Liu, W., Yang, H., Liwu, L., 2006. Hydrogen isotopic composition of n-alkanes from terrestrial plants correlate with their ecological life forms. Oceologia 150, 330–338.

März, C., Schnetger, B., Brumsack, H-J., 2010. Paleoenvironmental implications of Cenozoic sediments from the central Arctic Ocean (IODP Expedition 302) using inorganic geochemistry. Paleoceanography, 25, PA3206.

Merlivat, L., Jouzel, J., 1979. Global climatic interpretation of the Deuterium-Oxygen relationship for precipitation. Journal Geophysical Research 84, 5029–5033.

Müller, P. J., Kirst, G., Rohland, G., von Storch, I. & Rosell-Melé, A., 1998. Calibration of the alkenone paleotemperature index UK'37 based on core-tops from the eastern South Atlantic and the global ocean (60uN-60uS). Geochim. Cosmochim. Acta 62, 1757–1772.

Pagani, M., Pedentchouk, N., Huber, M., Sluijs, A., Schouten, S., Brinkhuis, H., Sinninghe Damsté J.S., Dickens, G.R., 2006. Arctic hydrology during global warming at the Palaeocene/Eocene thermal maximum. Nature, 442, 671-675.

Pearson, P. N., van Dongen, B.E., Nicholas, C.J., Pancost, R.D., Schouten, S., Singano, J.M., Wade, B.S., 2007. Stable warm tropical climate through the Eocene Epoch. Geology 35, 211-214.

Pearson, P.N., Palmer, M.R., 2000. Atmospheric carbon dioxide concentrations over the past 60 million years. Nature 406, 695–699.

Powers, L.A., Werne, J.P., Johnson, T.C., Hopmans, E.C., Sinninghe Damsté, J.S., Schouten, S., 2004. Crenarchaeotal membrane lipids in lake sediments: A new paleotemperature proxy for continental paleoclimate reconstruction? Geology, 32, 613-616.

Sachse, D., Radke, J., Gleixer, G., 2006. δD values of individual n-alkanes from terrestrial plants along a climatic gradient: Implications for the sedimentary biomarker record. Organic Geochemistry 37, 469-483.

Sauer, P.E., Eglinton, T.I., Hayes, J.M., Schimmelmann, A., Sessions, A.L., 2001. Compound-specific D/H ratios of lipid biomarkers from sediments as a proxy for environmental and climatic conditions. Geochim. Cosmochim. Acta 65, 213–-222.

Schouten, S., Hopmans, E.C., Schefuß, E. & Sinninghe Damsté, J.S., 2002. Distributional variations in marine crenarchaeotal membrane lipids: a new tool for reconstructing ancient sea water temperatures? EPSL 204, 265–274

Sessions, A.L., Burgoyne, T.W., Schimmelmann, A., Hayes, J.M., 1999. Fractionation of hydrogen isotopes in lipid biosynthesis. Organic Geochemistry 30, 1193–1200.

Sluijs, A., Brinkhuis, H., Schouten, S., Bohaty, S.M., John, C.M., Zachos, J.C., Reichart, G.J., Sinninghe Damsté, J.S., Crouch, E.M., Dickens, G.R., 2007. Environmental precursors to rapid light carbon injection at the Palaeocene/Eocene boundary. Nature 450, 1218–1221.

Speelman, E.N., van Kempen, M.M.L., Barke, J., Brinkhuis, H., Reichart, G.J., Smolders, A.J.P., Roelofs, J.G.M., Sangiorgi, F., de Leeuw, J.W., Lotter, A.F., Sinninghe Damsté, J.S., 2009a. The Eocene Arctic *Azolla* bloom: environmental conditions, productivity and carbon drawdown. Geobiology 7, 155-170.

Speelman, E.N., Reichart, G.J., de Leeuw, J.W., Rijpstra, W.I., Sinninghe Damsté, J.S., 2009. Biomarker lipids of the freshwater fern *Azolla* and its fossil counterpart from the Eocene Arctic Ocean. Organic Geochemisty 40, 628-637.

Speelman, E.N., Sewall J.O., Noone, D., Huber, M., von der Heydt, A., Sinninghe Damsté, J.S., Reichart, G.J. Modeling the influence of a reduced equator-to-pole sea surface temperature gradient on the distribution of water isotopes in the Eocene. EPSL, 298, 57-65.

Sternberg, L.D.L., 1988. D/H ratios of environmental water recorded by D/H ratios of plant lipids. Nature 333, 59–-61.

Waddell, L.M., and Moore, T.C., 2008. Salinity of the Eocene Arctic Ocean from oxygen isotope analysis of fish bone carbonate. Paleoceanography, 23, PA1S12.

Weijers, J.W.H., Schouten, S., Spaargaren, O.C., Sinninghe Damsté, J.S., 2006. Occurrence and distribution of tetraether membrane lipids in soils: Implications for the use of the TEX86 proxy and the BIT index. Organic Geochemistry 37, 1680–1693.

Weller, P., Stein, R., 2008 Paleogene biomarker records from the central Arctic Ocean (Integrated Ocean Drilling Program Expedition 302): organic carbon sources, anoxia, and sea surface temperature. Paleoceanography 23, PA1S17.

Yang, H., Equiza, A. M., Jagels, R., Pagani, M., Briggs, D., 2005. Carbon and hydrogen isotopic compositions of deciduous conifers under a continuous-light environment: implications for the interpretation of the high-latitudinal plant isotope record at the PETM. Oecologia, 160, 461-470.

Zhou, Y., Grice, K., Stuart-Williams, H., Farquhar, G.D., Hocart, C.H., Lu, H., Liu, W., 2010. Biosynthetic origin of the saw-toothed profile in $\delta^{13}C$ and $\delta^{2}H$ of n-alkanes and systematic isotopic differences between n-, iso- and anteiso-alkanes in leaf waxes of land plants. Phytochemistry, 71, 388-403.

Physiological and carbon isotopic responses of the freshwater fern *Azolla* to elevated pCO_2 conditions

Highly laminated sediments from the Arctic Ocean, from IODP expedition 302, contained intact microspore massulae and megaspores of the aquatic floating fern *Azolla*, indicating that *Azolla* grew and reproduced in situ. The coinciding timing of the *Azolla* interval with a shift towards heavier $\delta^{13}C$ values of planktonic and benthic organisms (due to higher primary productivity), a stratified Arctic Ocean (due to freshening of the surface waters) is interesting, since the freshwater fern could have contributed to reducing atmospheric carbon dioxide levels. Recently, the carbon isotopic composition of *Azolla* specific biomarkers has been reported for both the Eocene *Azolla* interval as for modern *Azolla*. The Eocene *Azolla* specific diols (-29,1‰ to -31,1‰) are enriched compared to extant Azolla biomarkers (-38,0‰ to -39,9‰). It has been suggested that this offset could have been caused by a different $\delta^{13}C$ composition of the Eocene atmosphere or by an effect of elevated pCO_2 on ($\varepsilon_{fixation}$). Here we test the influence of elevated pCO_2 conditions on physiological aspects and on the carbon isotopic composition of *Azolla*. *Azolla* specimens have been cultured under three controlled pCO_2 regimes and constant $\delta^{13}CO_2$. Results show that biomass production of *Azolla* increases under elevated pCO_2 concentrations, but that the total organic carbon content (TOC in %) is similar under all CO_2 treatments. Since the TOC follows the same trend as the biomass production, enhanced biomass production of *Azolla* under high CO_2 levels results in an enlarged TOC pool. The carbon isotopic composition of *Azolla* if not affected by different pCO_2 regimes. Under all pCO_2 treatments, the carbon isotopic fractionation during photosynthesis is equal ($\varepsilon_{(fixation)}$ ranges from -16 ‰ to -22‰). Since carbon fractionation does not seem to be influenced by pCO_2 concentrations, the $\delta^{13}C$ composition of *Azolla* is merely affected by the $\delta^{13}C$ composition of the atmospheric CO_2. As a consequence, the enriched $\delta^{13}C$ signal of Eocene *Azolla* biomarkers compared to their modern counterparts, can be explained by enrichment of the carbon isotope composition of the Eocene atmospheric carbon dioxide.

1. Introduction

Sediments from the central Arctic Ocean, IODP expedition 302, contained intact microspore massulae and megaspores of the aquatic floating fern *Azolla*, indicating that *Azolla* grew and reproduced in situ. The *Azolla* interval has been dated to Early/Middle Eocene age, from ~49.3 to ~48,1 Ma (Speelman *et al*, 2009a), when climatic conditions were substantially different from today's. Sea surface and air temperatures were higher throughout the Eocene (e.g. Pearson *et al*, 2007), with much warmer sea surface waters at the poles (e.g. Brinkhuis *et al*, 2006). Additionally, the equator-to-pole sea surface temperature (SST) gradient was reduced during the Eocene compared to today's (Bijl *et al*, 2009). Furthermore, enhanced greenhouse conditions prevailed at the start of the Cenozoic Era, with elevated atmospheric CO_2 concentrations, ranging between 400-3000 ppm (Pearson and Palmer, 2000). The timing of the Eocene *Azolla* event corresponds to a global shift in isotopic carbon (e.g. Zachos *et al*, 2001). The heavier $\delta^{13}C$ values, found in Eocene foraminifera, suggest that primary production was enhanced. When primary production is increased, surface waters become depleted in ^{12}C, since this carbon isotope is preferred in biosynthetic processes. The resulting ^{13}C enriched signal of the surface waters is reflected in the $\delta^{13}C$ values of planktonic (Waddell and Moore, 2008) and benthic organisms (Zachos *et al*, 2001). Interestingly,

enhanced primary production can reduce the atmospheric carbon dioxide content, by sequestrating atmospheric carbon in organic matter.

The occurrence of *Azolla* in the Eocene Arctic setting is remarkable, since extant *Azolla* can only grow in low saline environments (van Kempen *et al*, in press), suggesting that the input of freshwater in the Eocene Arctic surface ocean might have been increased. Available proxy data confirm that humidity was higher at the Eocene Arctic than at present (Jahren and Stenberg, 2003). Additionally, the hydrogen isotopic composition of the Arctic precipitation (δD) was enriched as suggested by modeling results (Speelman *et al*, in press) and validated by proxy-based δD reconstructions of the Early/Middle Eocene precipitation (Dekker, Master thesis part 1; Jahren *et al*, 2009). The hydrogen isotopic composition of the central Arctic surface waters, on the other hand, was much more depleted during the *Azolla* event, as a consequence of reduced mixing of the sea surface and deeper saline waters (Dekker, Master thesis part 1). The freshening of the surface waters combined with the deeper saline waters, resulted in a strong halocline in the Eocene Arctic Ocean (Waddell and Moore, 2008). The prevalence of a strong halocline, in combination with the highly laminated sediments from IODP expedition 302 (Brinkhuis *et al*, 2006), suggest that the Eocene Arctic basin was stratified. The stratification of the Arctic waters is furthermore illustrated by increased organic carbon accumulation rates (e.g. Knies *et al*, 2008) and the enrichment of trace metal elements as Co, Cu, Fe, Mo, V and Zn (e.g. März *et al,* 2010).

The production of *Azolla* in the stratified Arctic Ocean is interesting, since the freshwater fern could have contributed to reducing atmospheric carbon dioxide levels (Speelman *et al*, 2009a). *Azolla* makes use of atmospheric CO_2 for its carbon source. As a consequence, the production of *Azolla* sequestrates atmospheric CO_2 into organic matter. Under ambient CO_2 conditions, *Azolla* produces relative high amounts of biomass (amongst others Allen *et al*, 1988; Idso *et al*, 1989; Cheng *et al*, 2010). However, CO_2 concentrations in the Eocene are thought to have been enhanced. In theory, elevated pCO_2 conditions stimulate the biomass production of vegetation. The increased growth rate at elevated atmospheric CO_2 concentrations is the result of enhanced photosynthesis. The rate of photosynthesis is reliant on the rate of Rubisco (ribulose-1,5-biphosphate carboxylase/oxygenase) (Makina and Mae, 1999). The ratio between carboxylase and oxygenase depends on the ratio of the partial pressure of CO_2 and O_2 at the location of photosynthesis, inside the leaf. Since the partial pressure of carbon dioxide inside the leaves is in balance with the atmospheric pCO_2, the rise of the aerial CO_2 concentration stimulates the carboxylation part of the catalyses and suppresses the oxygenation (Makino and Mae, 1999). The stimulating effect of elevated pCO_2 concentrations on photosynthesis and biomass production varies among plant species (Ainsworth and Long, 2005), which may be associated with other limiting factors, such as nutrients (especially nitrogen and phosphorus). *Azolla* lives in close harmony with the N-fixating cyanobacteria *Anabaena Azollae* (Peters and Meeks, 1989). This way, *Azolla* can modulate its own nitrogen supply and plant species with symbiotic N-fixating bacteria often show a larger response to elevated atmospheric CO_2 concentrations than non-fixing species if other nutrients (such as K, P and H_2O, needed for optimal N-fixation) are not deficient (Lee *et al*, 2003, Cheng *et al*, 2010). The stimulating effect of elevated pCO_2 levels on the biomass production of *Azolla*, suggest that the freshwater fern could have been a major contributor to the carbon drawdown in the high pCO_2 Eocene.

Furthermore, specific biomarker lipids for *Azolla* have recently been found in both extant specimens and in the Eocene sediments (1,ω20 diols) (Speelman et al, 2009b). For both samples, the carbon

isotopic composition was determined, where the 1,ω20 diols from the Eocene showed a 8‰ enrichment compared to their modern counterparts (Speelman et al, 2009a). They reasoned that this offset could have been caused by a difference in biosynthetic pathways between Eocene and extant *Azolla*, a different $\delta^{13}C$ composition of the Eocene atmosphere or by an effect of elevated pCO_2 on ($\varepsilon_{fixation}$).

Speelman *et al* (2009b) tested the influence of elevated CO_2 conditions on *Azolla* by culturing *Azolla* under various atmospheric CO_2 regimes. Their pilot experiments showed an increase in the amount of *Azolla* biomass production at elevated pCO_2. The *Azolla* specimens yielded twice as much biomass under a pCO_2 of 1910 ppm (high[CO_2]) compared to a control treatment with a pCO_2 of 340 ppm (ambient[CO_2]). In addition, a substantial change was found in the bulk $\delta^{13}C$ values of *Azolla* under elevated CO_2 concentrations (Speelman, personal communicaton), with a more depleted carbon isotope signature under the high[CO_2] treatment. Unfortunately their experiments couldn't maintain constant levels of CO_2 inside the aquaria and they have not monitored the $\delta^{13}C$ signal of the atmospheric CO_2, vital to report the relation between pCO_2 levels and the isotopic fractionation between $\delta^{13}CO_2$ and (bulk) $\delta^{13}C$**.** As a consequence, the observed variation in $\delta^{13}C$ could not yet be explained and the difference between the $\delta^{13}C$ signal of Eocene Azolla biomarkers and their modern counterparts could not be explained.

The purpose of this study is to repeat the experiments by Speelman *et al* (2009b), while improving the CO_2 supply and monitoring the $\delta^{13}CO_2$. By culturing Azolla under a control pCO_2 (ambient CO_2), an intermediate pCO_2 (2x ambient CO_2) and a high pCO_2 regime (5x ambient CO_2), the influence of various pCO_2 concentrations on physiological aspects of the freshwater fern will be examined, as with the pilot experiments. The physiological focus will be on inspecting whether a high pCO_2, as presumably prevailed during the Eocene *Azolla* event, could have resulted in enhanced carbon assimilation. In addition, the effect of elevated CO_2 levels on the carbon isotopic composition of *Azolla* will be investigated, to better understand the offset between the Eocene and extant *Azolla* $\delta^{13}C$ signal.

2. Materials and Methods

2.1 Sample material

Extent *Azolla*

For the culturing experiment, *Azolla filiculoides* specimens were collected from an arable land ditch in the Netherlands.

2.2 Methods

2.2.1 Experimental set-up

To study the influence of various atmospheric CO_2 conditions on the growth of *Azolla*, three pCO_2 treatments were applied to the *Azolla* in quadruplicate. The *Azolla* were treated with either an ambient atmospheric CO_2 concentration [310 ppm] (a[CO_2]), an intermediate pCO_2 concentration [660 ppm] (i[CO_2]), or a high CO_2 concentration [1550 ppm] (h[CO_2]). The freshwater fern was grown under a 16/8 hour day-night cycle with a light intensity of 250 watt/m^2. A description of the experiment is outlined below and an additional schematic set-up is added to the supplementary information (A1).

The *Azolla* specimens were grown in airtight glass aquaria, with a water/air volume of 9,8 L/8,2 L. 18 L min^{-1} of air was blown through the headspace, with a gas outlet to balance the overflow of air (figure 1). The air supplied to the aquaria was a custom-made mixture of zero CO_2 air (with the use of a Sodalime scrubber) and regulated concentrations of CO_2 in synthetic air (Air Liquide; Eindhoven, the Netherlands), using mass flow controllers and gas blenders (Bronkhorst Hi-Tec, Veenendaal, the Netherlands). The atmospheric carbon dioxide concentrations in the supplied air were monitored daily, using an Infrared Gas Analyzer (IRGA, type ABB advance Optima, Ettenleur, the Netherlands) Since one of the objectives of this research was to track the isotopic fractionation of carbon during the biosynthesis of various lipids within *Azolla*, the $\delta^{13}C$ of the atmospheric CO_2 was monitored closely. One liter bulk samples were taken directly from the overflow air outlet and were reprocessed offline, after which the $\delta^{13}CO_2$ was measured using a dual-inlet mass spectrometer (SIRA-24 EM). The *Azolla* specimens were grown on a nutrient solution containing 1.75 mmol L^{-1} $NaHCO_3$, 1.75 mmol L^{-1} $CaCl_2 \cdot 2H_2O$, 0.025 mmol L^{-1} $NaH_2PO_4 \cdot H_2O$, 1 mmol L^{-1} K_2SO_4, 1 mmol L^{-1} $MgSO_4 \cdot 7H_2O$, 0.01 mmol L^{-1} Fe-EDTA, 0.001 $CuSO_4 \cdot 5H_2O$, 0.02 mmol L^{-1} $MnCL_2 \cdot 4H_2O$, 0.01 mmol L^{-1} $ZnSO_4 \cdot 7H_2O$, 0.003 mmol L^{-1} $NaMoO_4 \cdot 2H_2O$, 0.02 mmol L^{-1} H_3BO_3, 0.004 mmol L^{-1} $CoCl_2 \cdot 6H_2O$, with a pH of 8. The nutrient solution was supplied at a rate of 0,4 L h^{-1} from a stock solution, the water level inside the aquaria was held constant using an overflow outlet. The nutrient solution contained no nitrogen, making *Azolla* completely dependent on its cyanobacterial symbiont (*Anabaena Azollae*) for nitrogen. The limiting nitrogen conditions in the nutrient solution helped preventing the growth of algae, which compete with *Azolla* for other nutrients and light availability (van Kempen, personal communication). The nutrient solution were monitored every sampling for total inorganic carbon (TIC) and dissolved organic carbon (DOC) content.

At the start of the experiments 3 g of fresh *Azolla* was introduced into each aquarium. *Azolla* was sampled twice during the culturing experiments, on the 6^{th} and on the 11^{th} day. To estimate the growth rate under different pCO_2 regimes, the total fresh weight of the Azolla was determined after which 3 g of Azolla was put back into the aquaria during the first harvest. The rest of the fresh Azolla was oven dried at 70°C for 48 hours for the determination of dry weights and elemental isotopic composition.

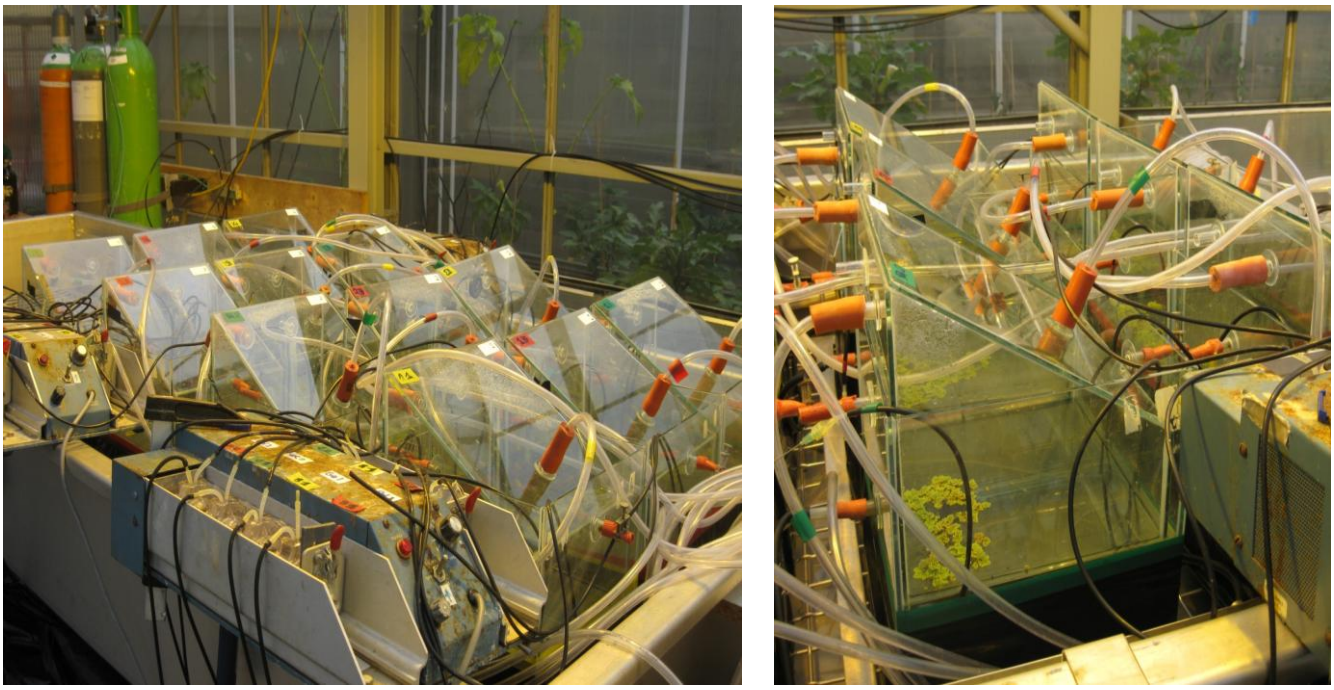

Figure 1. The photo on the left side displays the total experimental set-up. The close up photo on the right shows the location of the air supply (translucant tubes), nutrient supply (black tubes) and overflow outlets.

2.2.2 Cumulative dry weight measurements

To determine the growth rate of Azolla under different atmospheric pCO_2 regimes, the total dry weight at a specific sampling was calculated using the dry weight/ fresh weight ratio from a subsample. The Azolla specimens were oven dried at 70°C for 24 hours. Cumulative dry weights were based on using these dry weight ratios, adding them up to the total dry weight calculated for the previous time intervals.

2.2.3 Bulk $\delta^{13}C$, $\delta^{15}N$, TOC and N_{toc} measurements

The *Azolla* specimens were rinsed to remove contaminants and oven dried at 70°C for 24 hours, immediately after sampling. Bulk *Azolla* samples were measured in triplicates for all samples separately, for both the roots and leaves individually. Analyzes on the total organic carbon content (TOC), $\delta^{13}C_{TOC}$, total nitrogen content (N_{tot}) and $\delta^{15}N$ were performed using an elemental analyzer (Fison NA 1500 CNS), connected to a mass spectrometer (FInnigan Detla Plus). Isotopic values were measured against international standards (atropine), using Vienna Peedee Belemnite (VPDB; $\delta^{13}C$ = 0‰) to report the $\delta^{13}C_{TOC}$ values. $\delta^{15}N$ values are calculated as per mille excess above their natural abundance in air (Mariotti, 1983). Analytical precision was determined by comparison with international and in-house standards. Precision was better than 8% for TOC, 0,07‰ for $\delta^{13}C_{TOC}$, 1,9% for N_{tot} and 0,12‰ for $\delta^{15}N$.

2.2.4 Compound specific $\delta^{13}C$ measurements

The *Azolla* specimens were rinsed to remove contaminants and oven dried at 70°C for 24 hours, immediately after harvesting. Compound specific isotopic measurements were preformed on *Azolla* on all aquaria individually. Oven-dried *Azolla* samples were powdered and subsequently ultrasonically extracted using a dichloromethane (DCM):Methanol (MeOH) mixture (2:1, v/v) (5 times for 25 min). To separate the compounds of interest the extracts were separated by silica column

chromatography, using hexane [F1], DCM [F2], DCM:MeOH (20:1) [F3] and MeOH [F4] as subsequent eluents. The more polar fractions [F2, F3 and F4] were methylated with BF_3/MeOH at 60°C for 10 min (to convert acidic lipids in fatty acids methyl esters [FAME]) and silylated with BSTFA in pyridine at 60°C for 20 min (to convert the alcohols into the corresponding TMS-ethers). The components were indentified using gas chromatography/mass spectrometry (GC/MS) spectra (Thermo Trace GC Ultra, Thermo Fisher Scientific Inc.). Samples were on-column injected at 70°C, on a CP-sil 5CB fused silica column (30 m x 0.32 mm i.d., film thickness 0.1 µm) with helium as carrier gas set at constant pressure (100 KPa). The oven was programmed to 130°C at 20°C min^{-1} and then to 320°C at 4°C min^{-1}, followed by an isothermal hold for 20 min. Subsequently, compound specific $\delta^{13}C$ values were determined using isotope ratio monitoring gas chromatography-mass spectrometry (GC-IRMS), using a ThermoFinnigan Delta-Plus XP mass spectrometer. A similar column and over program was used as for the GC/MS measurements, though injection was performed using an autosampler (Gerstel MPS 2 twister) with a 10 ml syringe with 70mm needle length. The temperatures of the combustion and the reduction ovens were set to 940 °C and 630 °C, respectively. Co-injected squalane, with an offline determined isotopic composition was used as internal standard. Carbon isotopic compositions are reported against Vienna Peedee Belemnite and are based on duplicate analyses. In the case of methylated and silylated samples, the $\delta^{13}C$ values were corrected for the use of BF_3/MeOH and BSTFA.

3. Results and discussion

3.1 Growth rate at elevated CO_2 conditions

It is known that the biomass production of *Azolla* is relatively high under normal (ambient) conditions (Peters and Meeks, 1989). This is validated by the results of the culturing experiments discussed here (figure 2). The total biomass of Azolla is increased by 70% after 5 days and even by 165% after 10 days. In addition, higher CO_2 concentrations seem to increase the biomass production even more. After 10 days the total dry biomass per aquaria was 0,429 ± 0,06 g; 0,467 ± 0,04 g and 0,570 ± 0,08 g for the control (310 ppm), intermediate pCO_2 (660 ppm) and high pCO_2 (1550 ppm) treatments respectively. After the first sampling, *Azolla* cultured under high[CO_2] yielded 1.40 times more biomass than *Azolla* grown under control conditions ambient[CO_2] and *Azolla* biomass cultured under intermediate[CO_2] increased 1.16 times compared to the control. Although the measured growth rates are lower than the results by Speelman *et al* (2009b), the trend is analogous. In addition, previous research on the effects of elevated CO_2 concentrations on biomass production of various plant species is in agreement with the results shown here (e.g. Cheng *et al*, 2010; Ainsworth and Long, 2005; Vu, 2005; Kimball *et al*, 2002).

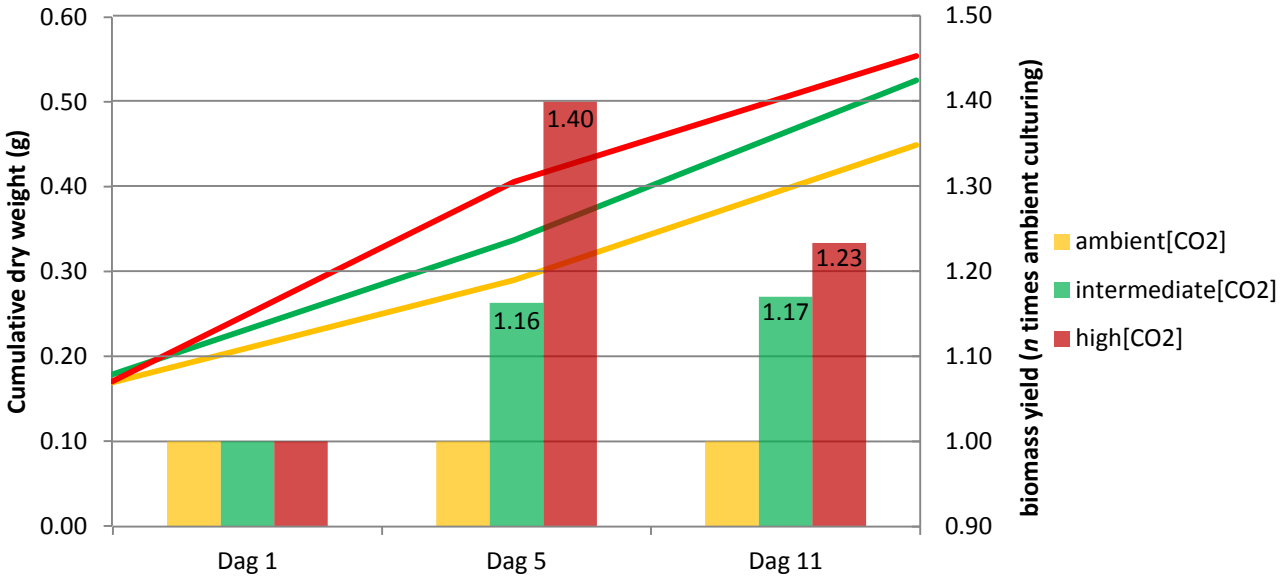

Figure 2. The average cumulative dry weight of Azolla during culturing and biomass yield of the Azolla specimens compared to the control (control set at 1.00)

Where the biomass yield for the intermediate[CO_2] treatment was constant throughout the whole experiment (at both sampling moments ~1.16 times more biomass was produced compared to the control), the biomass production rate in the high[CO_2] treatment was reduced after final sampling (figure 2) (with a yield of 1.40 times control for the first sampling and 1.23 times control for the final sampling). This difference is not caused by inconsistencies in the experimental set-up, since the CO_2 concentrations and nutrient availability were kept constant throughout the treatment (Appendix). Algal growth, on the other hand, could have been responsible for the decreased biomass yield, as the presence of algae was substantially increased in two of the aquaria under high pCO_2 regime. As an effect the biomass production rate in these aquaria was limited to 1.10 times the biomass yield under control conditions, whereas the growth rate of the other two aquaria was continuous throughout the experiment, with a biomass production rate of ~1.40 times control (the original dataset is visualized in the Appendix, A4).

3.2 Bulk TOC and N_{tot} measurements

The total organic carbon (TOC) of the *Azolla* species at the final sampling was similar for all three treatments (about 40%) (table 1). Although the TOC content slightly decreased with increasing carbon dioxide conditions, the TOC values are not substantially different. These results are in line with experimental results from Cheng *et al* (2010). Since the TOC follows the same trend as the biomass production (figure 2), enhanced biomass production of *Azolla* under high CO_2 levels results in an enlarged TOC pool.

In addition to the TOC, the total nitrogen content was also similar for all three treatments. This can be explained by the continuous addition of nitrogen by n-fixating bacteria (*Anabaena Azollae*), that life symbiotic in the leaf cavities of *Azolla*. Nitrogen production by n-fixating bacteria is increases under elevated pCO_2 conditions, provided that nutrients supporting the n-fixation are available (Van Groenigen *et al*, 2006)

Table 1. TOC and N_{tot} of Azolla, cultured under different pCO_2 treatments

	C content (%)	N content (%)
Ambient[CO2]	**42.83**±6.1	**2.76**±1.1
Intermediate[CO2]	**41.87**±5.2	**2.55**±0.6
High[CO2]	**40.96**±5.7	**2.59**±1.0

3.3 Bulk $\delta^{13}C$ measurements

The original *Azolla* specimens used for these experiments had a bulk $\delta^{13}C$ value of ~ -29‰ (table 2). This isotopic composition is the same as general bulk $\delta^{13}C$ values for C_3-plants (Hayes *et al*, 2001) and similar to prior reported $\delta^{13}C$ values for *Azolla* biomass (Speelman *et al*, 2009a).

After the experimental treatments, the bulk $\delta^{13}C$ value of *Azolla,* grown under controlled ambient conditions, was more depleted (-44.38 ±2.60‰ vs -28.98 ±0.33‰, table 2). This effect can be explained by a different isotopic composition of the atmosphere inside the aquaria ($\delta^{13}CO_2$) compared to the atmospheric $\delta^{13}C$ inside the greenhouse. The carbon isotopic composition of the air inside the headspaces was -25.7 ±0.6‰, -26.4 ±0.7‰ and -27.7 ±0.2‰ for the ambient[CO_2], intermediate[CO_2] and high[CO_2] treatments respectively, thus lighter than the $\delta^{13}CO_2$ of the air in which the original Azolla was grown (-16,8‰). The lighter $\delta^{13}CO_2$ values in the aquaria are due to the supply of air with a more negative $\delta^{13}CO_2$ from the gastank. In addition, the $\delta^{13}CO_2$ can be influenced by the contribution of respired CO_2 during the day (Lanigan *et al*, 2008). However, the effect of respiration on the isotopic composition of the atmosphere can be neglected here, since the air flow through the headspaces during the experiments was relatively fast. The rapid flow of CO_2 is validated by the relatively constant pCO_2 concentrations inside the aquaria throughout the experiments (310 ±50 ppm, 660 ±50 ppm, and 1550 ±230 ppm for the three treatments respectively). As a result the CO_2 produced by respiration was removed quite quick via the gas outlet.

Table 2. Bulk $\delta^{13}C$ of pre-cultured Azolla and after treatment with three different pCO_2. In addition the fractionation during photosynthesis for the three treatments is calculated.

	Bulk $\delta^{13}C$ (‰)	$\varepsilon_{(fixation)}$ (‰)
Azolla	**-28,98** ±0,33	-12,18
Ambient[CO2]	**-44,38** ±2,60	**-18,58**
Intermediate[CO2]	**-45,80** ±0,90	**-19,60**
High[CO2]	**-47,50** ±3,00	**-20,10**

The overall carbon isotopic composition of the biomass (bulk $\delta^{13}C$), is not only determined by the isotopic composition of the source CO_2, it is furthermore influenced by fractionation during the fixation ($\varepsilon_{(fixation)}$) of carbon (Hayes *et al*, 2001). By comparing the carbon isotopic composition of the source CO_2 and of the total biomass, an interpretation of the overall fractionation between $\delta^{13}CO_2$ and bulk $\delta^{13}C$ can be made. The second column in table 2 displays the $\varepsilon_{(fixation)}$ of the original *Azolla* and of the *Azolla* grown under different pCO_2 conditions. The $\varepsilon_{(fixation)}$ for the original Azolla specimens is substantially smaller than the fractionation by the *Azolla* specimens after culturing. This difference can be explained by fluctuating $\delta^{13}CO_2$ concentrations inside the greenhouse. Atmospheric

CO_2, in general, has a carbon isotopic composition of -8‰. As mentioned before, the atmospheric $\delta^{13}CO_2$ inside a greenhouse is affected by respiration (Lanigan *et al*, 2008), making the isotopic composition of the air more depleted. The air inside and outside the greenhouse were irregularly in contact through opened windows and doors, as a consequence the $\delta^{13}CO_2$ values inside the greenhouse will have fluctuated. At the time of measuring the $\delta^{13}CO_2$ was relatively negative, whereas it has probably been more positive throughout the growing period of the original *Azolla*. A more positive $\delta^{13}CO_2$ value increases the $\varepsilon_{(fixation)}$ of the original Azolla to values that are similar to the fractionation by the pCO_2 treated *Azolla* and values that are in line with fixation effects by C_3 plants in general (e.g. Hayes *et al*, 2001).

The results in table 2, suggest that the carbon dioxide levels in the atmosphere do not affect the fractionation of CO_2 during biomass production of Azolla, since values for $\varepsilon_{(fixation)}$ are similar for all three treatments (ranging from -16‰ to -22‰). This is in contrast to $\varepsilon_{(fixation)}$ values of other C_3 plants cultured under naturally elevated pCO_2 conditions (Miglietta *et al*, 1998; Sharma and Willams, 2008). They found a larger fractionation under higher pCO_2 levels, explained by a larger discrimination against ^{13}C during photosynthesis. In C_3 plants, the overall carbon isotopic fractionation ($\varepsilon_{(fixation)}$) can be broken down to the isotopic effect of CO_2 transport from the outside environment to the place of net photosynthesis (the leaves) and to the isotopic effect of CO_2 fixation by Rubisco (Hayes et al, 2001). When CO_2 concentrations are sufficiently high, the exchange of CO_2 between the source and the leaf cells is balanced. As a consequence the partial pressure of CO_2 outside and inside the leaves is equal, and the rate of CO_2 fixation is limited by the enzymatic reaction (Hayes et al, 2001). Additionally, when the concentration of CO_2 inside the leaf is high, the discrimination against ^{13}C is increased, because the lighter ^{12}C is preferable used in biological processes. As more ^{12}C is fixed in biomass, the bulk $\delta^{13}C$ values will be more negative (O'leary, 1981). However, this effect is not visible in the $\varepsilon_{(fixation)}$ values of Azolla. The observed spread in both the $\delta^{13}C$ and the $\varepsilon_{(fixation)}$ values can be explained by the sampling method, since all samples used for the bulk isotope measurements contain both original and new *Azolla* material. Appendix A4 shows the effects of this sampling method on the $\delta^{13}C$ values of the *Azolla* bulk material.

3.4 Compound specific $\delta^{13}C$ measurements

The carbon isotopic composition of bulk biomass material is merely a representation of the average $\delta^{13}C$ composition of plants. In addition to the isotopic fractionation during the incorporation of CO_2 via the process of photosynthesis (as discussed in section 3.3), synthesis of specific lipids is also associated with isotopic effects. Different lipid compound classes are produced via distinct biosynthetic pathways (figure 3, based on fig 1 from Chikaraishi *et al*, 2004) and will therefore have varying $\delta^{13}C$ signals.

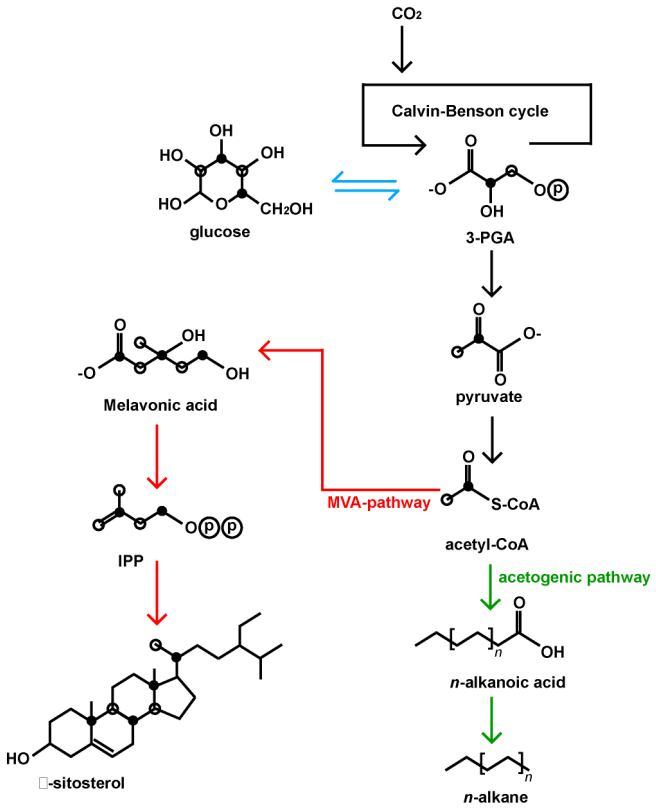

Figure 3. A scheme illustrating the incorporation of CO_2 in various compound classes following different pathways.

For example, monosaccharide units (sugars) are enriched in ^{12}C compared to bulk $\delta^{13}C$ values (Van Dongen *et al*, 2002; Teece and Fogel, 2007; Dungait *et al*, 2008). Monosaccharide compounds are formed directly from the end-products of the Calvin-Benson cycle. Sugars are used as an energy source for the production of other lipid compounds, and the biosynthesis of these lipid compounds is accompanied with fractionation effects, altering the original $\delta^{13}C$ value. The process of glycolysis transforms glucose into pyruvate, which in turn is decarboxylated to acetyl-CoA, a C_2 compound used in the formation of various lipids (figure 3) N-alkanoic acids (fatty acids) are produced following the acetogenic pathway, using acetyl-CoA as a precursor. β-sitosterol, on the other hand, is produced according to the MVA pathway (Lichtenhaler *et al*, 1997), where acetyl-CoA is first transformed to mevalonic acid, a key precursor for isoprenoid lipids. As a consequence of the fractionation effect during the synthesis of these lipids and during the production of each intermediate component (as acetyl-CoA), the $\delta^{13}C$ signal gets more depleted. Table 3 displays the $\delta^{13}C$ values for a selection of several compound classes for the original *Azolla* (adapted from Speelman *et al*, 2009b). The carbon isotopic composition of all compounds are more depleted than bulk $\delta^{13}C$, which is in line with reported $\delta^{13}C$ values in various of C_3 plants (e.g. Chikaraishi *et al*, 2004). The distinctive variations between the carbon isotopic signal of various compound classes with respect to bulk $\delta^{13}C$ values follow the same trend among all plant species, however absolute $\delta^{13}C$ values vary among different plant classes. This effect can be attributed to species specific kinetic isotopic effects of key biochemical reactions of each plant class (Chikaraishi *et al*, 2004).

Table 3. The $\delta^{13}C$ values (‰ vs. VPDB) for selected lipids in extant Azolla extracts

Compound	$\delta^{13}C$ (‰)	Compound	$\delta^{13}C$ (‰)	Compound	$\delta^{13}C$ (‰)
1,11 C_{30} diol	-39,1			C_{45} wax ester	-38,9
1,13 C_{32} diol	-38,0	C_{32} OHFAME	-39,0	β-sitosterol	-32,6
1,15 C_{34} diol	-38,7	C_{34} OHFAME	-39,1	C_{16} fatty acid	-34,5
1,17 C_{36} diol	-39,9	C_{36} OHFAME	-40,7	C_{18} fatty acid	-36,0
				TOC	-30,3

As discussed in section 3.3, the overall fractionation ($\varepsilon_{(fixation)}$) is similar for *Azolla* specimens cultured under different pCO_2 concentrations, ranging from -16‰ to -22‰. The observed spread in $\delta^{13}C$ values from the experiments is even larger than the variations between selected compounds in table 3. As a consequence, any effects of elevated CO_2 levels on the compound specific fractionation will be undetectable within the spread of $\delta^{13}C$ values.

3.5 Implications for the Eocene climate

Recently, specific biomarker lipids for Azolla have been found in both extant *Azolla* as in the Eocene sediments. A series of wax lipids has been identified with a characteristic hydroxyl group at the ω20 position; the ω20 alkanols, mid-chain ω20 hydroxy FA and 1,ω20 diols (Speelman *et al*, 2009a). These straight chain components are thought to be biosynthesized via the same pathway as they all have similar chain length distributions and virtually identical $\delta^{13}C$ values. (Speelman *et al*, 2009a). The characteristic hydroxyl group suggests that all three compound classes have a related precursor, presumably a parent secondary alcohol.

The carbon isotopic composition of the *Azolla* specific biomarkers in extant *Azolla* ranged between -38‰ and -39,9‰ (Speelman et al, 2009b). In contrast, the $\delta^{13}C$ value of the 1,ω20 diols from the Eocene Arctic sediments is about 8‰ enriched (Speelman et al, 2009a). This offset has been ascribed to a different $\delta^{13}C$ composition of the Eocene atmosphere or to an effect of elevated pCO_2 on ($\varepsilon_{fixation}$). The results shown in this thesis propose that the latter reason could be discarded as well, since ($\varepsilon_{fixation}$) seems not to be affected by elevated pCO_2 concentrations. With this in mind, the difference between the $\delta^{13}C$ composition of Eocene and modern *Azolla* compounds is merely affected by the $\delta^{13}C$ composition of the atmospheric CO_2. Since the $\delta^{13}C$ of the Eocene 1,ω20 diols is about 8‰ enriched, it suggests that the carbon isotopic signal of the Eocene atmosphere was also isotopically heavier. Enriched $\delta^{13}C$ values for the Eocene atmospheric CO_2 have been reported earlier (e.g. Hayes et al, 1999), though they reported Eocene $\delta^{13}CO_2$ values of only 3‰ heavier. As the large (8‰) enrichment is not recognized in other $\delta^{13}CO_2$ records, the enriched signal of the Eocene *Azolla* biomarkers might be explained by other factors. The discrepancy between 3‰ and 8‰ might be attributed to a difference in biosynthetic pathways between Eocene and extant *Azolla*, however this seems unlikely as the distribution of *Azolla* specific diols in both Eocene and extant *Azolla* is similar (Speelman et al, 2009a). Diagenetic effects on the 1,ω20 diols could also have changed the isotopic composition, although the preservation of diols is better than that of other lipid compounds (Speelman et al, 2009a). Another explanation could be that *Azolla* specimens make use of bicarbonate (from the surface waters) as an alternative carbon source. As bicarbonate has on average a more negative $\delta^{13}C$ signal, the incorporation of this carbon source declines the bulk $\delta^{13}C$ composition of *Azolla*. Unfortunately it is not yet proven whether *Azolla* could make use of this carbon source.

4. Conclusion

The experiments presented in this thesis confirm that biomass production of *Azolla* is increased under elevated pCO_2 concentrations. Additionally, organic carbon accumulation is similar under all CO_2 levels, suggesting that enhanced biomass production of *Azolla* under high CO_2 levels results in an enlarged TOC pool. The carbon isotopic composition of *Azolla* does not seems to be affected by different pCO_2 regimes. Under all pCO_2 treatments, the carbon isotopic fractionation during photosynthesis is equal ($\varepsilon_{(fixation)}$ ranges from -16 ‰ to -22‰). In addition to isotopic fractionation during photosynthesis, the $\delta^{13}C$ value of specific compounds is influenced by fractionation effects during the synthesis of these components. Different compound classes in *Azolla* have a different $\delta^{13}C$ signal as the consequence of being synthesized via diverse pathways (Speelman *et al*, 2009a). The variation between various compounds classes, however, is smaller than the observed spread in $\delta^{13}C$ values from the different CO_2 treatments. As a consequence effects of elevated CO_2 levels on the compound specific fractionation will be undetectable within the spread of $\delta^{13}C$ values. Since the carbon isotopic composition of *Azolla* is not influenced by different pCO_2 levels, the earlier reported difference between the $\delta^{13}C$ composition of Eocene and modern *Azolla* compounds (Speelman *et al*, 2009a) is merely affected by the $\delta^{13}C$ composition of the atmospheric CO_2. The $\delta^{13}C$ of *Azolla* specific diols from the Eocene sediments are 8‰ more enriched compared to the $\delta^{13}C$ of extant *Azolla*, suggesting that the Eocene $\delta^{13}CO_2$ should have been more enriched by the same amount. However an enrichment of only 3‰ is (until now) recognized in other Eocene $\delta^{13}CO_2$ records. To find a plausible explanation for the offset in $\delta^{13}CO_2$ values, more research needs to be done.

Appendix

A 1. Scheme of the experimental set-up

Figure A1 schematically illustrates the experimentsal set-up. The squares represent the aquaria, where each color corresponds to a different treatment. Each aquaria is continuously supplied with nutrient solution, pumped up from a stock solution using two motors. Water level is kept constant by an overflow outlet. The supplied air is a mixture of zero CO_2 atmospheric air and pure CO_2 from a gas tank, controlled by mass flow controllers and gas blenders. The air is supplied continuously to each aquaria by two inflow points and overflow pressure is released by an outlet point.

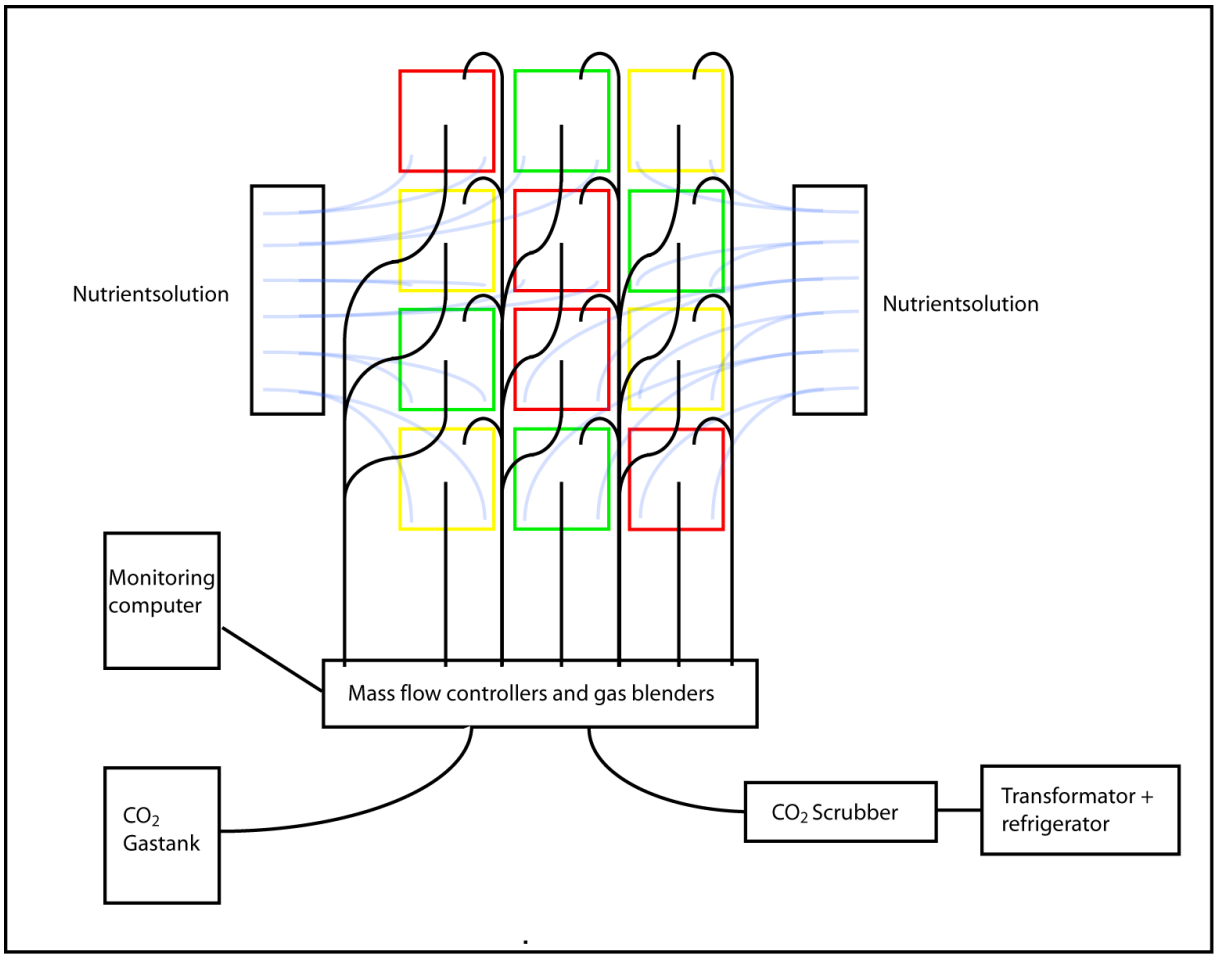

Figure A1. A schematic plan of the experimental set-up.

A 2. Time series pCO2

Figure A2 shows the monitored CO_2 and $\delta^{13}CO_2$ of the three treatments. The CO_2 was measured for each aquarium individually, whereas the $\delta^{13}CO_2$ was measured for one aquaria only. Both stay relatively continuous throughout the duration of the experiment, This suggests that the resulting differences on physiological aspects and carbon isotopic of *Azolla* between the three treatments are only due to the effect of different atmospheric CO_2 levels to *Azolla*.

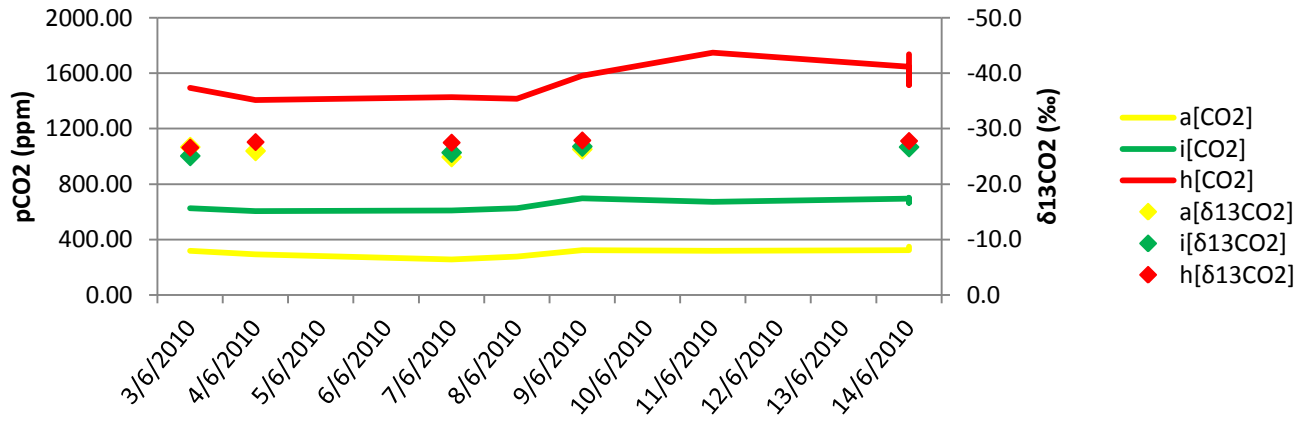

Figure A2. The average pCO_2 concentrations and $\delta^{13}CO_2$ values of the three treatments over the experimental duration

A 3. Growth rates versus the presence of algae

Figure A3 represents the growth rate of each aquarium individually. Although the variation between the various aquaria is large, the overall growth rates of *Azolla* cultured under elevated CO_2 concentrations are increased. The columns illustrate the biomass yield for each aquarium in relation to the control treatment. As with the growth rates, the variation is quite large. As described in the discussion, *Azolla* specimens from two aquaria, grown under a high CO_2 treatment (red columns), have a lower biomass accumulation compared to the other two. An explanation for this difference could be the relative abundance of algae (indicated by the blue line). After final sampling the presence of algae in each aquarium was rated compared to the other aquaria. *Azolla* specimens in two of the high CO_2 treatment aquaria were relatively overgrown with algae compared to the other aquaria. Algae compete with the *Azolla* for light availability and nutrients, affecting the growth rate of *Azolla*.

The algal abundance in one of the intermediate treatments (green columns), in contrast, was relatively low, keeping ideal growth conditions for the freshwater fern. The absence of algae is reflected in the biomass production by *Azolla* in this aquarium, which is relatively high compared to the other growth rates of *Azolla* under intermediate treatment.

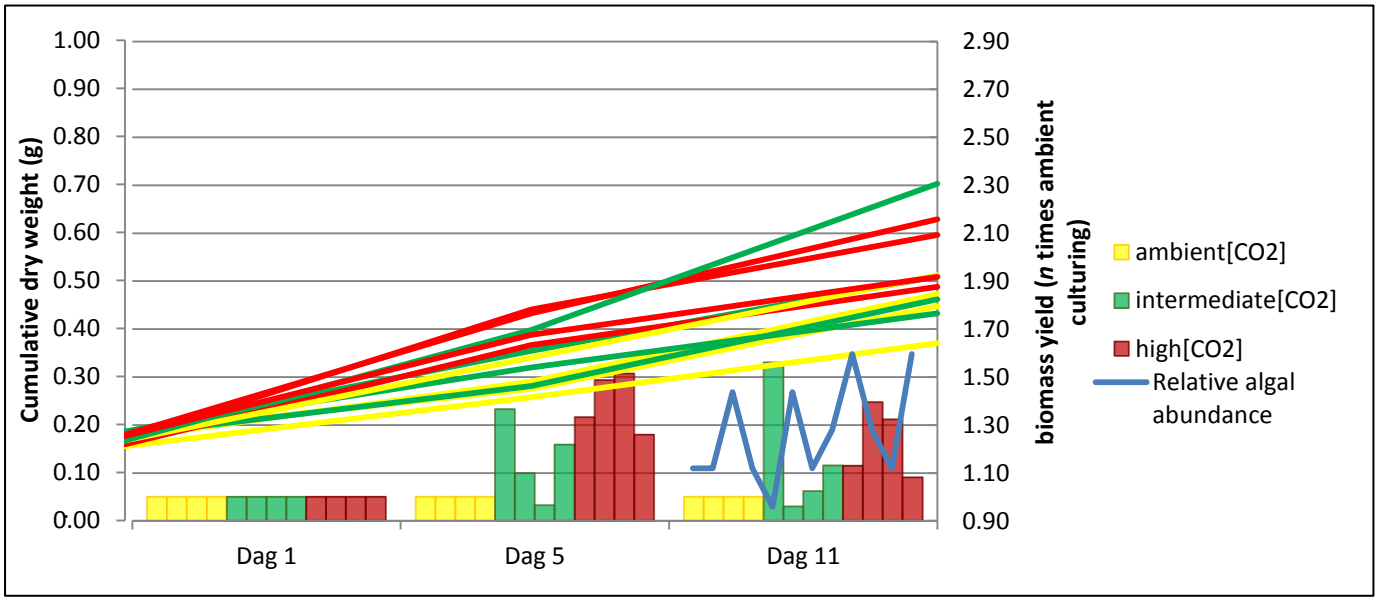

Figure A3. The cumulative dry weight of Azolla during culturing of each aquaria individually and biomass yield of the Azolla specimens compared to the control (control set at 1.00). Blue line represents relative algal abundance

A 4. Differences between new and old material

The samples used for the bulk $\delta^{13}C$ measurements are a combination of both original *Azolla* material and new *Azolla* material, grown under the three pCO_2 treatments. Table A….shows the average percentages of original and new material. Using these percentages, the average $\delta^{13}C$ value per treatment and the $\delta^{13}C$ signal of the original material, the actual $\delta^{13}C$ value of the new material could be calculated (table A…).

Table A… The percentages of original and new Azolla material, and the accompanying $\delta^{13}C$ and fractionation values

	$\delta^{13}C$ total (‰)	**original material (%)**	**new material (%)**	**$\delta^{13}C$ original (‰)**	**$\delta^{13}C$ new material (‰)**	**$\varepsilon_{(fixation)}$ new (‰)**
Ambient [CO2]	-44,38	41,00	59,00	-28,98	-55,64	-29,94
Intermediate [CO2]	-45,91	40,46	59,54	-28,98	-57,83	-31,43
High [CO2]	-46,84	30,55	69,45	-28,98	-55,18	-27,48

However, the new values for $\delta^{13}C$ and $\varepsilon_{(fixation)}$ are implausible. The very negative values here do not even fall in the range of the bulk $\delta^{13}C$ data presented in table 2. From this we can say that the bulk $\delta^{13}C$ data presented in table 2 is a plausible representation of the actual $\delta^{13}C$ signal of the cultured *Azolla*. Furthermore, measurements on individual leaves, show a carbon isotope composition similar to the powdered bulk $\delta^{13}C$ values (table A…), although slightly more negative. This difference can be explained by a different lipid composition of the leaves compared to the whole plant.

Table A… The carbon isotopic composition of individual leaves and powdered material

	$\delta^{13}C$ powdered samples (‰)	**$\delta^{13}C$** Individual leaves (‰)
Ambient [CO2]	-44,38 ±2,60	-46,64 ±3,75
Intermediate [CO2]	-45,91 ±0,90	-48,94 ±1,50
High [CO2]	-46,84 ±3,00	-49,93 ±3,15

References

Ainsworth, E.A., Long, S.P., 2005. What have we learned from 15 years of free-air CO2 enrichment (FACE)? A meta-analytic review of the responses of photosynthesis, canopy properties and plant production to rising CO2. New Phytologist, 165, 351-371 .

Allen, S.G., Idso, S.B., Kimball, B.A., Anderson, M.G., 1988. Relationship between growth rate and net photosynthesis of Azolla in ambient and elevated CO_2 concentrations. Agriculture, Ecosystems and environment, 20, 137-141.

Bijl, P.K., Schouten, S., Sluijs, A., Reichart, G.J., Zachos, J.C., Brinkhuis, H., 2009. Early palaeogene temperature evolution of the southwest Pacific Ocean. Nature 461, 776-779.

Brinkhuis, H., Schouten, S., Collinson, M.E., Sluijs, A., Sinninghe Damsté, J.S., Dickens, G.R., Huber, M., Cronin, T.M., Onodera, J., Takahashi, K., Bujak, J.P., Stein, R., van der Burgh, J., Eldrett, J.S., Harding, I.C., Lotter, A.F., Sangiorgi, F., van Konijnenburg-van Cittert, H., de Leeuw, J.W., Matthiessen, J., Backman, J., Moran, K.The Expedition 302 Scientists, 2006. Episodic fresh surface waters in the Eocene Arctic Ocean. Nature 441, 606–609.

Cheng, W., Sakai, H., Matsushima, M., Yagi, K., Hasegawa, T., 2010. Response of floating aquatic fern Azolla filiculoides to elevated CO_2, temperature, and phosphorus levels. Hydrobiologica, 656, 5-14.

Chikaraishi, Y., Naraoka, H., Poulson, S.R., 2004. Hydrogen and carbon isotopic fractionations of lipid biosynthesis among terrestrial (C3, C4 and CAM) and aquatic plants. Phytochemistry, 65, 1369-1381.

Dungait, J.A.J., Docherty, G., Straker V., Evershed, R.P., 2008. Interspecific variation in bulk tissue, fatty acid and monosaccharide d13C values of leaves from a mesotrophic grassland plant community. Phytochemistry, 69, 2041-2051.

Hayes, J.M., 2001. Fractionation of carbon and hydrogen isotopes in biosynthetic processes. Stable Isotope Geochemistry, 43, 225-277.

Hayes, J.M., Strauss, H., Kaufman, A.J., 1999. The abundance of 13C in marine organic matter and isotopic fractionation in the global biogeochemical cycle of carbon during the past 800 Ma. Chemical Geology, 161, 103–125.

Idso, S.B., Allen, S.G., Anderson, M.G., Kimball, B.A., 1989. Atmospheric CO_2 enrichment enhances survival of Azolla at high temperatures. Evironmental and experimental botany, 29, 337-341.

Jahren, A.H., Sternberg, L.S.L., 2003. Humidity estimate for the middle Eocene Arctic rain forest. Geology 31, 463-466.

Jahren A.H., Byrne, M.C.,Graham, H.V., Sternberg, L.S.L., Summons, R.E., 2009. The environmental water of the middle Eocene Arctic: Evidence from δD, $\delta^{18}O$ and $\delta^{13}C$ within specific compounds. Palaeogeogr., Palaeoclimatol., Palaeoecol. 271, 96-103.

Kimball, B.A., Kobayashi, K., Bindi, M., 2002. Responses of agricultural crops to free-air CO_2 enrichment. Advances in Agronomy, 77, 293-368.

Knies, J., Mann, U., Popp, B.N., Stein, R., Brumsack, H-J., 2008. Surface water productivity and paleoceanographic implications in the Cenozoic Arctic Ocean. Paleoceanography, 23, PA1S16.

Lanigan, G.J., Betson, N., Griffiths, H., Seibt, U., 2008. Carbon Isotope Fractionation during Photorespiration and Carboxylation in Senecio. Plant Physiology, 148, 2013–2020.

Lee, T.D., Tjoelker, M.G., Reich P.B., Russelle, M.P., 2003. Contrasting growth response of an N2-fixing and non-fixing forb to elevated CO2: dependence on soil N supply *Plant and Soil,* 255, 475–486.

Lichtenthaler, H.K., Rohmer, M., Schwender, J., 1997. Two independent biochemical pathways for isopentenyl diphosphate and isoprenoid biosynthesis in higher plants. Physiologica Plantarum 101, 643-652.

März, C., Schnetger, B., Brumsack, H-J., 2010. Paleoenvironmental implications of Cenozoic sediments from the central Arctic Ocean (IODP Expedition 302) using inorganic geochemistry. Paleoceanography, 25, PA3206.

Makino A., Mae. T., 1999. Photosynthesis and Plant Growth at Elevated Levels of CO2. *Plant Cell Physiol,* 40, 999-1006.

Mariotti A., 1983. Atmospheric nitrogen is a reliable standard for natural ^{15}N abundance measurements. Nature 303, 685-687.

Miglietta, F., Betlarini, I., Rashi, A., Körner, C., Vaccari, F.P., 1998. Isotope discrimination and photosynthesis of vegetation growing in the Bossoleto CO_2 spring. Chemophere, 36, 4-5.

O'Leary, M.H, 1981. Carbon Isotope fractionation plants. Phytochemistry, 20, 553-567.

Peters G.A., Meeks, J.C., 1989. The Azolla-Anabaena symbiosis: basic biology. Annual Review of Plant Physiology and Plant Molecular Biology, 40, 193-210.

Pearson, P. N., van Dongen, B.E., Nicholas, C.J., Pancost, R.D., Schouten, S., Singano, J.M., Wade, B.S., 2007. Stable warm tropical climate through the Eocene Epoch. Geology 35, 211-214.

Pearson, P.N., Palmer, M.R., 2000. Atmospheric carbon dioxide concentrations over the past 60 million years. Nature 406, 695–699.

Sharma, S., Williams, D.G., 2009. Carbon and oxygen isotope analysis of leaf biomass reveals contrasting photosynthetic responses to elevated CO2 near geologic vents in Yellowstone National Park. Biogeosciences, 6, 25–31.

Speelman, E.N., van Kempen, M.M.L., Barke, J., Brinkhuis, H., Reichart, G.J., Smolders, A.J.P., Roelofs, J.G.M., Sangiorgi, F., de Leeuw, J.W., Lotter, A.F., Sinninghe Damsté, J.S., 2009a. The Eocene Arctic Azolla bloom: environmental conditions, productivity and carbon drawdown. Geobiology 7, 155-170.

Speelman, E.N., Reichart, G.J., de Leeuw, J.W., Rijpstra, I.C., Sinninghe Damsté, J.S., 2009b. Biomarker lipids of the freshwater fern *Azolla* and its fossil counterpart from the Eocene Arctic Ocean. Organig Geochemistry, 40, 628-637.

Speelman, E.N., Sewall J.O., Noone, D., Huber, M., von der Heydt, A., Sinninghe Damsté, J.S., Reichart, G.J., 2010. Modeling the influence of a reduced equator-to-pole sea surface temperature gradient on the distribution of water isotopes in the Eocene. EPSL, 298, 57-65.

Teece, M.A., Fogel, M.L., 2007. Stable carbon isotope biogeochemistry of monosaccharides in aquatic organisms and terrestrial plants. Organic geochemistry, 38, 458-473.

Van Dongen, B.E., Schouten, S., Sinninghe Damsté, J.S., 2002. Carbon isotope variability in monosaccharides and lipids of aquatic algae and terrestrial plants. Marine Ecology Progress Series, 232, 83-92.

Van Groenigen, K.J., Six, J., Hungate, B.A., De Graaff, M.A., Van Breemen, N., Van Kessel, C., 2006. Element interactions limit soil carbon storage. Proceedings of the National Academy of Sciences of the United States of America, 103, 6571-6574.

Vu, J.C.V., 2005., Photosynthesis, Growth, and Yield of Citrus at Elevated Atmospheric CO_2. Journal of Crop Improvement, 13, 361-376.

Waddell, L.M., and Moore, T.C., 2008. Salinity of the Eocene Arctic Ocean from oxygen isotope analysis of fish bone carbonate. Paleoceanography, 23, PA1S12.

Zachos, J.M., Scott, L.D., Lohmann, K.C., 1994. Evolution of early Cenozoic marine temperatures. Paleoceanography 9, 353-387.

Acknowledgement

First I would like to thank Eveline N. Speelman and Gert-Jan Reichart for their ideas and guidance through this project. This research used samples and data provided by the Integrated Ocean Drilling Program (IODP), funding for this research was provided by the DARWIN centre for Biogeology, Utrecht University and StatoilHydro.

Special thanks go out to Monique van Kempen and the University of Nijmegen for providing the materials for the pCO_2 culturing experiments and for helping me to optimize the experimental conditions. Furthermore I would like to thank Arnold van Dijk, Jan Kubiak and Anita van Leeuwen for their technical laboratory assistance. Last but not least, I would like say thanks for the opportunity to present my result on the EGU 2010.